Volume 28 Number 17 15 October 2008 ISSN 0278-4343

ELSEVIER

CONTINENTAL SHELF RESEARCH

Research Papers

L. Zhai, J. Sheng and R.J. Greatbatch — 2357 Baroclinic dynamics of wind-driven circulation in a stratified bay: A numerical study using models of varying complexity

C.M. Aiken, M.I. Castillo and S.A. Navarrete — 2371 A simulation of the Chilean Coastal Current and associated topographic upwelling near Valparaíso, Chile

J. Guillén, S. Soriano, M. Demestre, A. Falqués, A. Palanques and P. Puig — 2382 Alteration of bottom roughness by benthic organisms in a sandy coastal environment

L. Gao, D.-J. Li and P.-X. Ding — 2393 Variation of nutrients in response to the highly dynamic suspended particulate matter in the Changjiang (Yangtze River) plume

J.S. Patil and A.C. Anil — 2404 Temporal variation of diatom benthic propagules in a monsoon-influenced tropical estuary

H.-H. Zhang, G.-P. Yang and T. Zhu — 2417 Distribution and cycling of dimethylsulfide (DMS) and dimethylsulfoniopropionate (DMSP) in the sea-surface microlayer of the Yellow Sea, China, in spring

M.M. Robinson and R.A. McBride — 2428 Anatomy of a shoreface sand ridge revisited using foraminifera: False Cape Shoals, Virginia/North Carolina inner shelf

A.N. Green, M. Ovechkina and R. Uken — 2442 Nannofossil age constraints for the northern KwaZulu-Natal shelf-edge wedge: Implications for continental margin dynamics, South Africa, SW Indian Ocean

X. Guo and A. Valle-Levinson — 2450 Wind effects on the lateral structure of density-driven circulation in Chesapeake Bay

T.P. Sampere, T.S. Bianchi, S.G. Wakeham and M.A. Allison — 2472 Sources of organic matter in surface sediments of the Louisiana Continental margin: Effects of major depositional/transport pathways and Hurricane Ivan

(*Continued on outside back cover*)

www.elsevier.com/locate/csr

Continental Shelf Research 28 (2008) 2450–2471

Contents lists available at ScienceDirect

Continental Shelf Research

journal homepage: www.elsevier.com/locate/csr

Wind effects on the lateral structure of density-driven circulation in Chesapeake Bay

Xinyu Guo [a,*], Arnoldo Valle-Levinson [b]

[a] Center for Marine Environmental Studies, Ehime University, 2–5 Bunkyo-Cho, Matsuyama 790-8577, Japan
[b] Department of Civil and Coastal Engineering, University of Florida, 365 Weil Hall, P.O. Box 116580, Gainesville, FL 32611, USA

ARTICLE INFO

Article history:
Received 10 August 2007
Received in revised form
25 March 2008
Accepted 20 June 2008
Available online 27 June 2008

Keywords:
Chesapeake Bay
Estuarine circulation
Wind-driven currents
Wind-induced mixing
Transverse structure

ABSTRACT

The response of the density-driven circulation in the Chesapeake Bay to wind forcing was studied with numerical experiments. A model of the bay with realistic bathymetry was first applied to produce the density-driven flow under average river discharge and tidal forcing. Subsequently, four spatially uniform wind fields (northeasterly, northwesterly, southwesterly, and southeasterly) were imposed to examine the resulting cross-estuary structure of salinity and flow fields. In general, northeasterly and northwesterly winds intensified the density-driven circulation in the upper and middle reaches of the bay, whereas southeasterly and southwesterly winds weakened it. The response was different in the lower bay, where downwind flow from the upper and middle reaches of the bay competed with onshore/offshore coastal flows. Wind remote effects were dominant, over local effects, on volume transports through the bay entrance. However, local effects were more influential in establishing the sea-level slopes that drove subtidal flows and salinity fields in most of the bay. The effect of vertical stratification on wind-induced flows was also investigated by switching it off. The absence of stratification allowed development of Ekman layers that reached depths of the same order as the water depth. Consequently, bathymetric effects became influential on the homogeneous flow structure causing the wind-induced flow inside the bay to show a marked transverse structure: downwind over the shallow areas and upwind in the channels. In the presence of stratification, Ekman layers became shallower and the wind-induced currents showed weaker transverse structure than those that developed in the absence of stratification. In essence, the wind-driven flows were horizontally sheared under weak stratification and vertically sheared under stratified conditions.

1. Introduction

The influence of winds on estuarine circulation (gravitational circulation) has been described for several decades. For example, the analytical solution of estuarine circulation given by Hansen and Rattray (1965) included the contribution of winds. According to their solution, a down-estuary wind intensified the estuarine circulation, while an up-estuary wind weakened it. Geyer (1997) applied this solution to explain observations in Waquoit Bay, Massachusetts, in terms of wind forcing. In addition, Weisberg (1976), Elliott (1978) and Wang (1979) also observed predominant wind-driven pulses in currents or sea levels of an estuary.

Recent studies have focused, in addition to the vertical and along-estuary structure of estuarine flows, on their transverse structure. Assuming a balance between pressure gradient and vertical stress divergence in an idealized estuary with a triangular cross-section, Wong (1994) and Friedrichs and Hamrick (1996) obtained an analytical solution for the circulation. The solutions in Wong (1994) are for flows driven by along-estuary density gradients, by local along-estuary winds, and by subtidal sea-level oscillations at the entrance to an estuary, which represent the remote effect of winds. His solutions revealed a marked transverse structure that depended on the bathymetry. In the deep central part of the triangular section, the net flow was in the opposite direction of the density gradient or the local winds. Over the two shallow sides of the cross-section, the net flow was in the direction of the density gradient or of the local winds. The current caused by a subtidal sea-level oscillation at the entrance to an estuary (the remote effect) was in the same direction throughout the cross-section but strongest in the deep central part.

Kasai et al. (2000) introduced rotation effects to the formulation of Wong (1994) and also looked at the transverse dynamics. They used the Ekman number to evaluate the relative importance of friction and rotation in their analytical solution. A large Ekman number meant that most of the water column was occupied by the Ekman depth. In that case, friction dominated the dynamics

* Corresponding author. Tel./fax: +81 89 927 9824.
E-mail address: guoxinyu@dpc.ehime-u.ac.jp (X. Guo).

0278-4343/$ - see front matter © 2008 Elsevier Ltd. All rights reserved.
doi:10.1016/j.csr.2008.06.008

and the current structure approached the solution given by Wong (1994), i.e., bathymetry causes a strong transverse structure in the currents. In the case of a small Ekman number, the solution approached the traditional two-layer vertical structure of estuarine circulation. Valle-Levinson et al. (2003) extended the solution of Kasai et al. (2000) to a section with arbitrary bathymetry and applied the solution to explain the transverse structure of observed currents in several estuaries with different Ekman numbers. Following the same dependence on the Ekman number, Winant (2004) and Sanay and Valle-Levinson (2005) characterized the wind-driven flows affected by Coriolis under various bathymetric cross-sections and homogeneous density.

The above theoretical studies have examined current structures inside the estuary and assumed a linear superposition of the wind-induced and density-induced currents. This, of course, differs in a real estuary because winds can change the density field as well as the turbulence field. Winds can change the strength of estuarine currents, while turbulence, according to Kasai et al. (2000) and Valle-Levinson et al. (2003), can change the transverse structure of the current, regardless of whether it is wind induced or buoyancy induced. Chao (1988) investigated the wind effects on a pre-existing estuarine current in an idealized estuary using a three-dimensional model, which included the effects of winds on the density field but neglected wind effects on the turbulence field because he used a constant viscosity.

In this study, the work of Guo and Valle-Levinson (2007) is extended through the inclusion of winds. A uniform wind field from four directions (NW, NE, SE, and SW) as well as the corresponding sea-level change at the bay mouth were prescribed in a numerical model of the Chesapeake Bay to examine the modifications to a pre-existing estuarine circulation inside the bay and at the bay mouth. These modifications were also assessed by determining the wind response in a homogeneous Chesapeake Bay.

2. Numerical model and experiments

The model used in this study is the same as in Guo and Valle-Levinson (2007), the Princeton Ocean Model (POM). The POM is a three-dimensional primitive equation ocean model that includes full thermodynamics and a Mellor-Yamada level 2.5 turbulence closure model (Mellor, 2004). The model domain and bathymetry are shown in Fig. 1. The horizontal resolution was 1/240° in both the zonal and meridional directions, which gave 744 grids in the meridional direction and 420 grids in the zonal direction. In the vertical, 11 sigma-levels were evenly distributed. Calculations with 21 sigma-levels showed qualitatively the same results as those with 11 sigma-levels. The minimum water depth in the model domain was set to 3 m. The time step was 3 s for the external mode and 120 s for the internal mode. During calculations, the vertical eddy viscosity and diffusivity were determined by the Mellor-Yamada turbulence closure model with a background value of $10^{-5}\,m^2/s$. At the bottom, a common quadratic friction law was used to calculate bottom stress (see Guo and Valle-Levinson, 2007 for the parameters used). The horizontal eddy viscosity was calculated by the embedded Smagorinsky formula with a proportionality parameter of 0.1, and the horizontal eddy diffusivity was obtained using an inverse Prandtl number of 0.5.

The model was first forced with river discharge, an ambient coastal current and tides to produce the estuarine currents in the Chesapeake Bay. The water temperature was set as a constant (15 °C) throughout all the calculations and only the evolution of salinity was calculated. The contribution of temperature to the density gradient in the horizontal and vertical directions has been

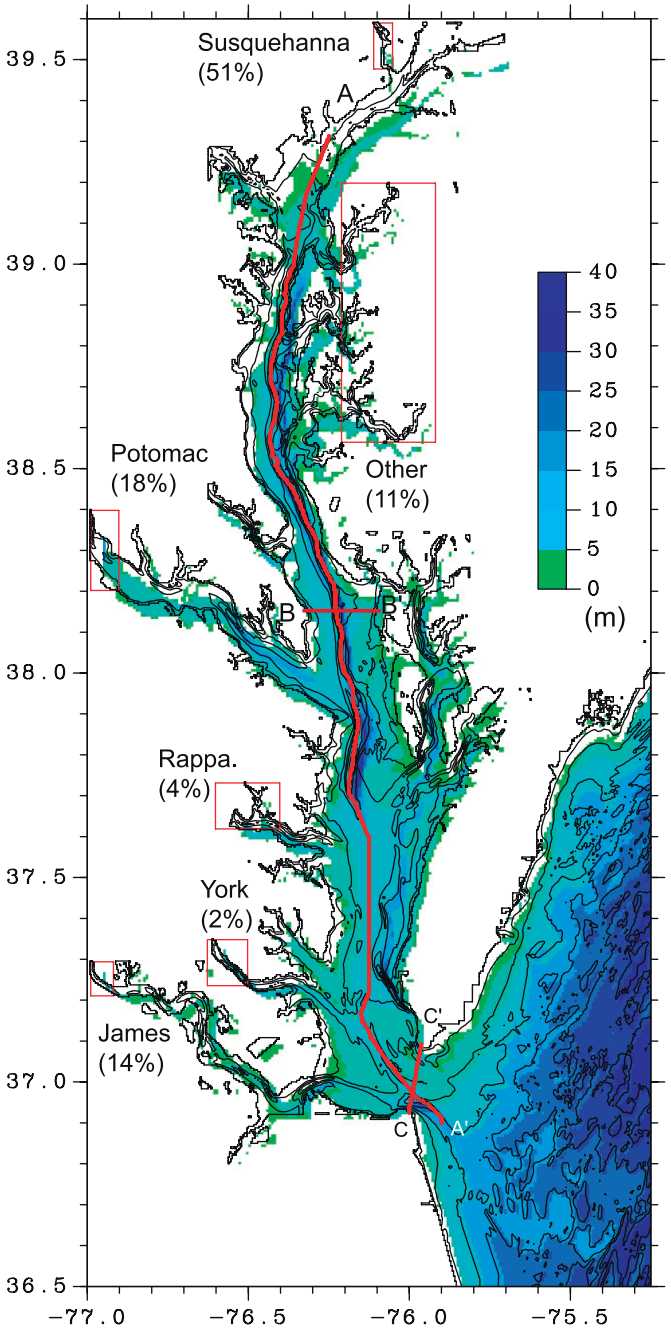

Fig. 1. Model bathymetry: the boxes denote river locations and the numbers inside the parentheses denote the percentage of each river discharge, relative to the total ($2200\,m^3/s$), as given by Hargis (1980). The longitudinal cross-section (A–A′) and two lateral cross-sections (B–B′ and C–C′) are referenced in subsequent figures.

suggested to be less than 1/4 relative to salinity (Seitz, 1971; Goodrich et al., 1987). Referring to Hargis (1980), a total of $2200\,m^3/s$ of fresh water was introduced to the model domain from the Susquehanna (51% of total), Potomac (18%), James (14%), Rappahannock (4%), York (2%), and other small rivers (11%) (see Fig. 1 for the position of the rivers and see Guo and Valle-Levinson, 2007 for the method of introducing river discharge).

Prescription of the southward ambient current in the shelf was motivated by previous studies. Beardsley and Boicourt (1981) reported a southward coastal current in the Middle Atlantic Bight. Epifanio and Garvine (2001) inferred the existence of a southward coastal current outside the Chesapeake Bay. In our simulations, an

ambient coastal current was imposed with a speed of 10 cm/s along the eastern boundary from 37.7°N to 38°N. Furthermore, it has been shown that the inclusion of an ambient current is essential for a realistic representation of the buoyant plume outside the bay (Guo and Valle-Levinson, 2007). The prescription of tidal currents is crucial to emulate the transverse structure of subtidal currents inside the bay and to represent the outflow plume path outside the bay (Guo and Valle-Levinson, 2007). Every simulation was forced with semidiurnal tides. In all the calculations, the results were saved hourly and the intratidal variability was removed with a low-pass tide killer filter (Hanawa and Mitsudera, 1985). The calculated tide and tidal currents are given by Guo and Valle-Levinson (2007). The open boundary conditions are specified in the same way as in the subroutine BCOND in POM (see Mellor, 2004 for a detailed description of this subroutine), which can directly include tidal currents, ambient current and sea-level change. Along the eastern open boundary, the tidal currents and ambient current are linearly superposed.

With the above configurations, the model was started with a constant salinity (32) in the entire domain and run for 246 days to obtain the estuarine circulation in the bay. Then a spatially uniform wind was imposed to the fundamental estuarine circulation to examine its response. Winds from four directions (northeasterly or 45°T, northwesterly or 315°T, southwesterly or 225°T, and southeasterly or 135°T) were imposed to the model from day 247 to 249. After that the winds stopped but the model simulation continued to day 265. During the 3 days of wind blowing, the magnitude of wind stresses was ramped-up from zero to the maximum during the first 12 h and was ramped-down from the maximum to zero in the final 12 h. Consequently, the magnitude of wind stress was kept maximum for 2 days, from day 247.5 to 249.5. The sea-level change due to the winds was calculated by the formula given in Fig. 4d of Paraso and Valle-Levinson (1996) and the calculated values were prescribed along the open boundary to examine the remote effects of winds. Essentially, a total of nine different cases were calculated as shown in Table 1, where case 0 is a control experiment with no winds; cases 1–4 are designed to examine the local wind effects and cases 5–8 are designed to examine the remote wind effects. Additional experiments 1H–4H were to examine the local wind effects in the absence of stratification and 1C–4C were to examine the combination of local and remote wind effects. The maximum magnitude of the wind stress in cases 1–8 was the same, 0.14 Pa. The calculations with half of this magnitude did not show essential difference in the results. The magnitude, direction, and duration of winds used here were determined from the analysis by Paraso and Valle-Levinson (1996) in Chesapeake Bay and from wind records during observations of the currents at the bay entrance (Valle-Levinson et al., 2001).

3. Results

3.1. Estuarine circulation

The salinity and subtidal currents obtained for the control case have been reported in Guo and Valle-Levinson (2007). Those results are described again, briefly, for a comparison with the results of the cases with winds. Surface salinity shows a typical distribution in an estuary (Fig. 2a). The along-estuary salinity gradient is greatest between the head of the bay and the intersection between the Potomac River and the main axis of the bay, and also at the bay entrance. In the transverse direction, salinity is relatively low along the western side and high along the eastern side, which is explained by the position of the rivers and the effects of Earth's rotation. Over the shelf outside the bay, the salinity is approximately 32, which is the same as the initial salinity and that prescribed along the open boundary. The only low salinity area outside the bay is near the bay entrance and is related to the outflow plume.

In general, the surface subtidal currents inside the bay are toward the ocean (Fig. 2b). Their speed is ~20 cm/s in the upper and middle bay, where the transverse salinity difference across the narrow sections is ~2–3. Surface subtidal flow is ~10 cm/s in the lower bay and increases again at the bay entrance. Outside the bay, two southward currents can be found. One is the imposed ambient current, north of the bay entrance, and the other is the outflow plume.

The transverse salinity gradient displayed at the surface (Fig. 2a) extends throughout the water column, as shown in a mid-bay section (Fig. 3c) and the bay entrance (Fig. 3e). The subtidal flow normal to the mid-bay section concentrates in the central part, with outflow in the upper layer and inflow underneath, both of which exceed 15 cm/s (Fig. 3d). The interface between opposite currents is almost flat. At the bay entrance (Fig. 3e), the lower salinity area at the southern side of the section corresponds to the outflow plume (Fig. 2a). The subtidal flow normal to the section concentrates in the Chesapeake Channel, with an outflow in the upper layer and an inflow in the lower layer (Fig. 3f). There is also an outflow in the upper layer and an inflow underneath in the North Channel but weaker than the exchange flows in the Chesapeake Channel. These subtidal flow features in the Chesapeake and North channels at the bay entrance are remarkably similar to the observations described in Valle-Levinson et al. (1998, 2001).

Transverse variability in subtidal flows is more apparent at the bay entrance (Fig. 3f) than in the mid-bay (Fig. 3d). This is indicated by the interface between opposite flows, which slopes downward to the south in the Chesapeake Channel. Such interface slope and transverse variability are attributed to tidal forcing, which produces stronger mixing in the lower bay than in the middle of the bay (Guo and Valle-Levinson, 2007).

Table 1
Wind stress and sea level applied at the model's open boundary

	Case								
	0	1	2	3	4	1H	2H	3H	4H
Eastward component (Pa)	0	−0.1	0.1	0.1	−0.1	−0.1	0.1	0.1	−0.1
Northward component (Pa)	0	−0.1	−0.1	0.1	0.1	−0.1	−0.1	0.1	0.1
Sea level (cm)	0	0	0	0	0	0	0	0	0
		5	6	7	8	1C	2C	3C	4C
Eastward component (Pa)		0	0	0	0	−0.1	0.1	0.1	−0.1
Northward component (Pa)		0	0	0	0	−0.1	−0.1	0.1	0.1
Sea level (cm)		26.9	−5.3	−26.9	5.3	26.9	−5.3	−26.9	5.3

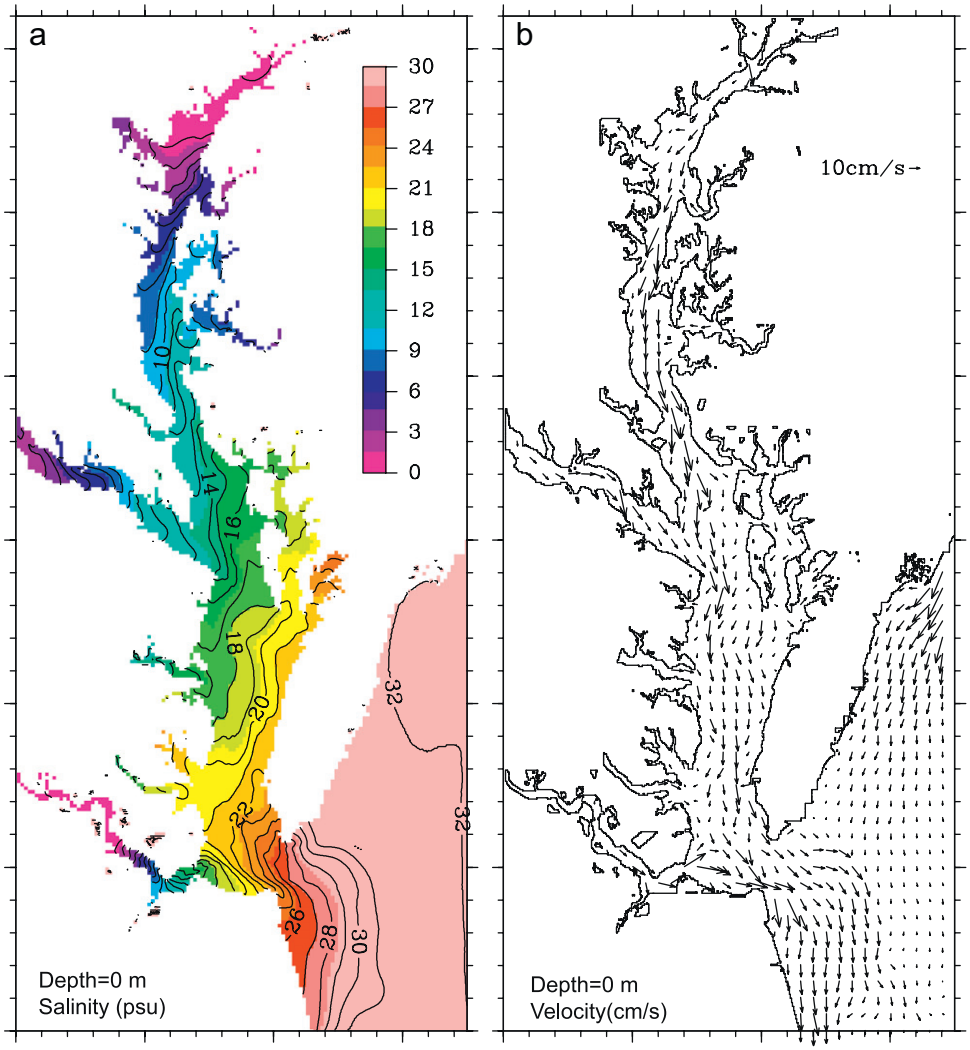

Fig. 2. Horizontal distribution of surface: (a) salinity and (b) velocity calculated for the control case (case 0).

3.2. *Response of density-driven circulation to winds: surface layer after 2 days*

As described in Section 2, a spatially uniform wind was imposed to the pre-existing estuarine circulation in the Chesapeake Bay to examine its effects on the salinity, subtidal currents, and turbulence fields. In this and the following sections, results are reported at the mature state (day 249.5), i.e., after the winds have blown at maximum speed for 2 days. Section 3.4 describes the response of the pre-existing estuarine circulation to sea-level change at bay mouth, i.e., remote wind effects. Section 3.5 describes the temporal response of water exchange through the bay entrance during the duration of the wind pulses in cases 1–6 (local or remote effects separately) and in cases 1C–2C (combination of local and remote effects).

The wind-induced changes in subtidal sea level are shown first (Fig. 4) because they have been extensively studied (e.g., Wang, 1979; Valle-Levinson et al., 2001, 2002). Under northeasterly winds (case 1; Fig. 4a), the sea level tilts upward from the upper bay to the lower bay by ~0.2 m. Also, sea level shows negative slopes across the lower bay, i.e., sea level decreases from the southwest to the northeast in the lower bay. This is a consequence of water piling up on the southwestern corner of the lower bay, as observed by Valle-Levinson et al. (2001, their Fig. 3) under northeasterly winds. Under northwesterly winds (case 2; Fig. 4b), the sea level also slopes upward from the upper to the lower bay by ~0.2 m. This feature is also consistent with the northwesterly wind pulse caused by Hurricane *Floyd* in 1999 (see Fig. 3 in Valle-Levinson et al., 2002). Under southwesterly winds (case 3; Fig. 4c), the sea level tilts upward from the southwestern corner of the bay toward the upper bay, as observed in Valle-Levinson et al. (2001). Finally, under southeasterly winds (case 4; Fig. 4d), the sea level slopes upward from the bay entrance to the upper bay, showing an inverse response to northwesterly winds. This is also in agreement with observations of Salas-Monreal and Valle-Levinson (2008). The sea-level responses produced by the model are qualitatively the same as those observed. The magnitude of the slopes is underestimated in the model by 5–30%, relative to observations with comparable winds, because of the remote effects as will be shown in Section 3.4 and the inverse barometer effect (Salas-Monreal and Valle-Levinson, 2008). Nonetheless, the shape and approximate magnitude of the sea-level slopes is consistent with observations for all wind directions.

The general features in the salinity field (Fig. 5) such as low salinity in the upper bay and high salinity in the lower bay are maintained for all wind cases. This suggests that the observed decrease of salinity in the entire bay during the passage of the Hurricane *Floyd* (Valle-Levinson et al., 2002) resulted not only from winds but also from the increased freshwater supply.

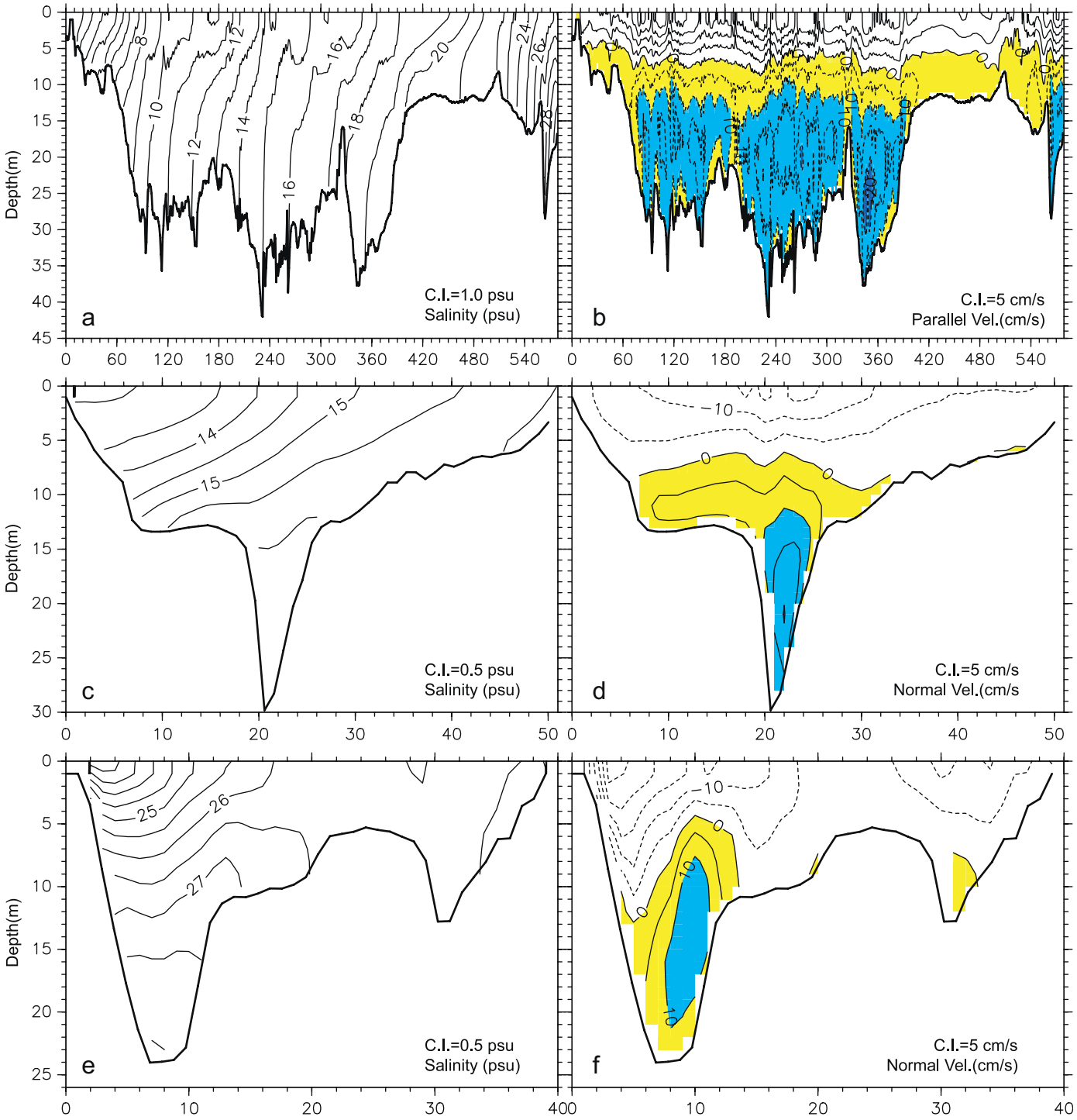

Fig. 3. Vertical distribution of salinity (left panels) and velocity (right panels) along Section A (top panels), Section B (middle panels) and Section C (lower panels). The velocity in (b) is the along-estuary component (parallel to Section A). Positive values denote currents toward the mouth of the bay. The velocity in (d) is the component normal to Section B and negative values denote current toward the mouth of the bay. The velocity in (f) is the component normal to Section C and negative values denote outflow from the bay entrance. The units shown on the abscissa represent the model grid number.

Northeasterly winds cause a decrease of salinity along the western coast and an increase along the eastern coast in the upper and middle bays (Fig. 5a). This response is seen by an elongation of isohalines in the north–south direction because of downwelling along the western coast and upwelling along the eastern coast. Hence, advective effects seem to dominate the wind response over diffusive effects (vertical mixing) in this part of the bay. Vertical mixing, were to dominate, would increase the surface salinity along both western and eastern coasts. Northeasterly winds seem to cause small changes in surface salinity in the lower bay but they do change the salinity distribution outside the bay. The downwind transport associated with the northeasterly wind drives low salinity water southward of the bay entrance, along the coast, consequently narrowing the outflow plume. Northwesterly winds drive water out of the bay and consequently the salinity inside the bay must decrease. However, the salinity in

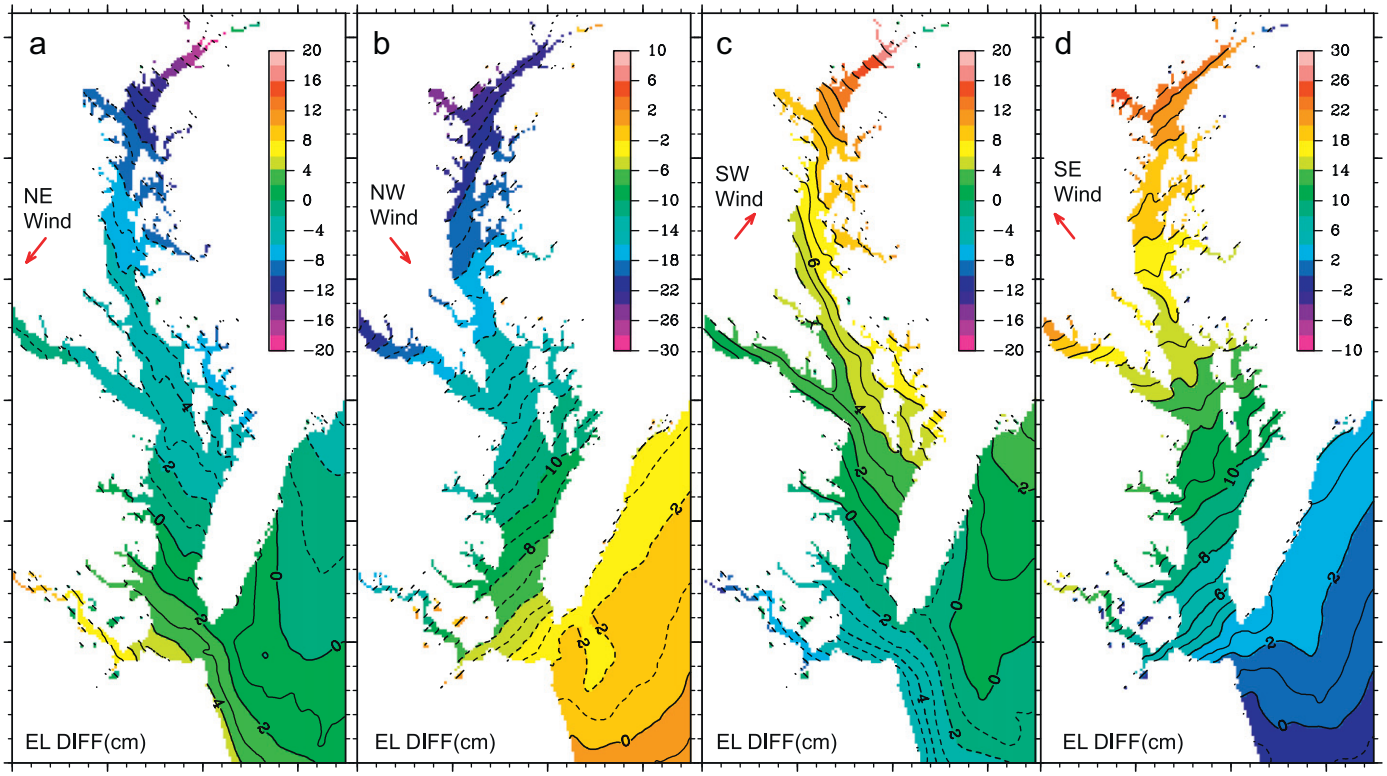

Fig. 4. Anomaly of sea level between cases 1–4 and case 0.

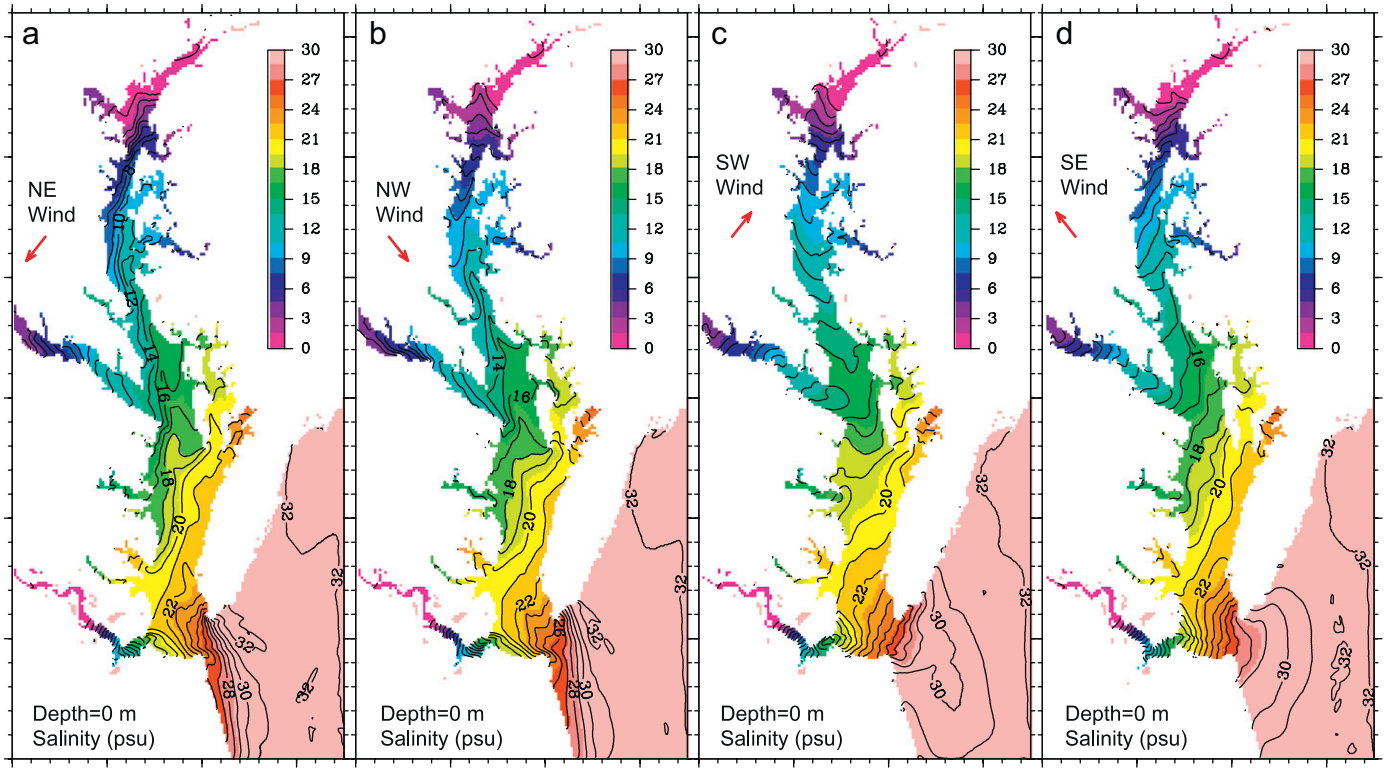

Fig. 5. Horizontal distribution of surface salinity calculated for cases 1–4.

the upper and middle bay decreases only slightly and that in the lower bay has no apparent change (Fig. 5b). This is likely caused by upwelling on the eastern coast and downwelling on the western coast in the upper bay plus the rebound of water outside the bay. Details on the responses of exchange flux through the bay entrance to the winds will be presented in Section 3.5. Outside the bay, the low-salinity area has a similar distribution to that in the case of northeasterly winds.

Southwesterly winds tend to reverse the sign of the east–west salinity gradient in the upper and middle bay (Fig. 5c). In this case, the salinity becomes higher along the western coast than along the eastern coast because of downwelling along the eastern coast and upwelling along the western coast. As in other cases, the salinity in the lower bay shows little change but outside the bay it shows a marked change in the structure of the plume (Fig. 5c). The outflow plume is detached from the coast to the south of the bay entrance and moves eastward and slightly northward. Southeasterly winds tend to weaken, relative to the control case, the east–west salinity gradient in the upper and middle bays but preserve the sign (Fig. 5d). Again, the salinity in the lower bay changes little but outside the bay it is noticeably modified.

The subtidal currents in the surface layer are sensitive to the wind direction (Fig. 6). In the upper and middle bay, northeasterly winds strengthen the surface outflow along the western coast (Fig. 6a). Outside the bay, northeasterly winds drive a coherent current structure by combining the ambient flow with the buoyant coastal current from the plume (Fig. 6a). Northwesterly winds intensify the outflow inside the bay and the outflow plume outside the bay (Fig. 6b). This intensification of the plume flow is caused by the convergence of the southward ambient flow at the outflow plume (Fig. 6b). Southwesterly winds dramatically hinder the surface outflow inside the bay but enhance the outflows from the Potomac and James Rivers to the main stem of Chesapeake Bay (Fig. 6c). Outside the bay, the outflow plume detaches from the coast to the south of the bay entrance while eastward outflow emanates from the bay entrance (Fig. 6c). Southeasterly winds hamper the surface outflow inside the bay and even produce opposite currents in the eastern portion at mid-bay (Fig. 6d). Outside the bay, a northward current appears offshore of the bay entrance, which collides with the ambient southward current at approximately 37.5°N (Fig. 6d).

Qualitatively, the response to wind of the subtidal surface currents (Fig. 6) can be interpreted as the combination of the currents following the wind direction (Hansen and Rattray, 1965; Geyer, 1997), and that normal to the wind direction (Chao, 1988; Fong and Geyer, 2001). The former is apparent in the upper and middle bay, where northwesterly winds reinforce the surface outflow while southeasterly winds weaken it. The latter is apparent outside the bay. Through the combination of onshore Ekman transport and sea-level setup near the coast, northeasterly winds produce a coherent southwestward current along the coast. Consequently, part of the coastal water is pushed into the bay and the outflow plume from the bay entrance is slenderized. Southwesterly winds, in contrast, cause a withdrawal of water out of the bay and a detachment of the outflow plume from the coast to the south of the bay entrance.

The lower bay shows a relatively insensitive response to wind forcing when compared to the bay as a whole. This is because the currents following the wind direction and those normal to the wind direction compete with each other there. For example, northeasterly winds drive water from the upper to the lower bay while they also drive coastal water into the lower bay, opposing the southward flows from the upper bay. As will be shown in Section 3.5, the initial response to northwesterly winds, for instance, is that the water inside the bay flows out. However, as the sea-level distribution shown in Fig. 4b is established, the flushing slows down and coastal water begins to enter the bay. Then the lower bay goes back to the state prior to wind forcing.

3.3. *Response of density-driven circulation to winds: vertical structure after 2 days*

The effect of winds on the vertical structure of salinity and subtidal currents under bathymetric variations is illustrated at a cross-section in the middle of the bay (Fig. 7) and at the bay entrance (Fig. 8). In the middle of the bay, northeasterly winds cause a westward migration and straightening of isohalines in the

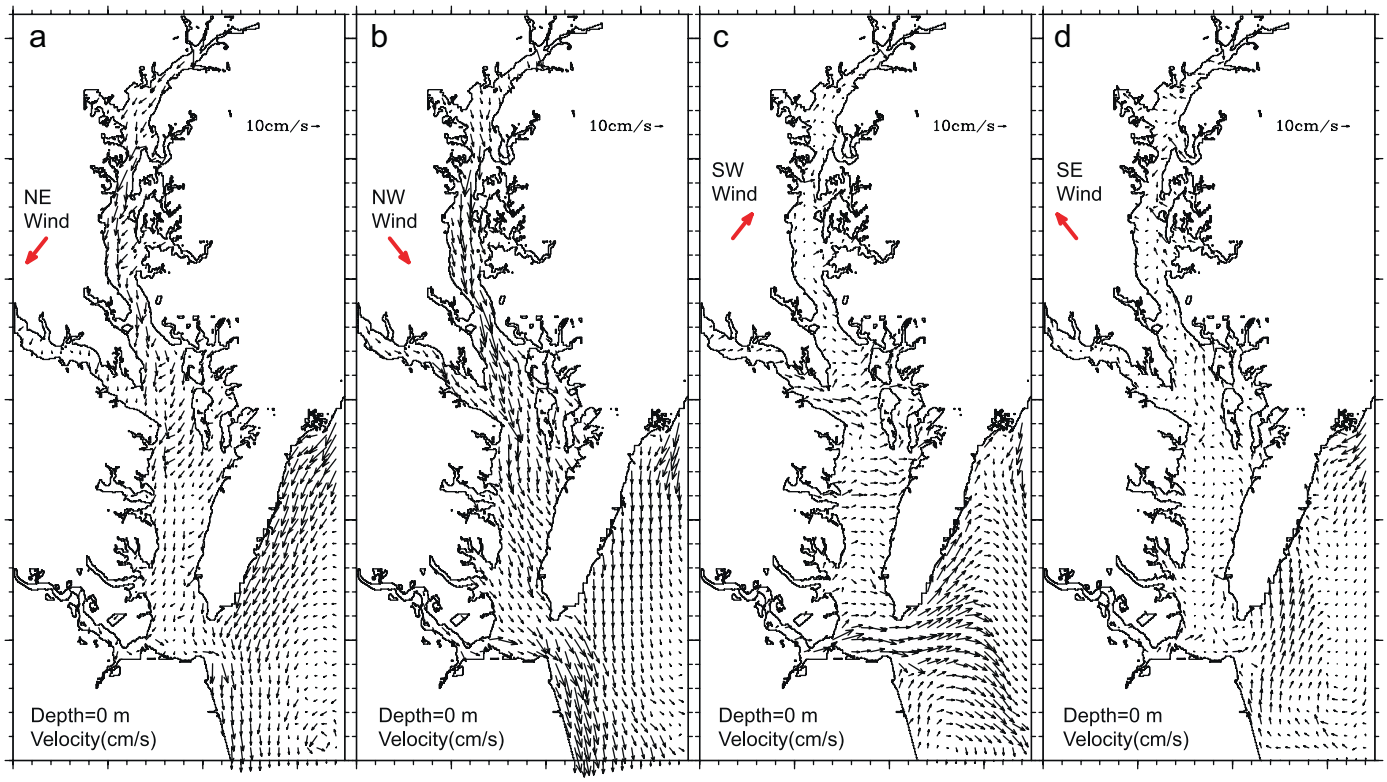

Fig. 6. Horizontal distribution of surface velocity calculated for cases 1–4.

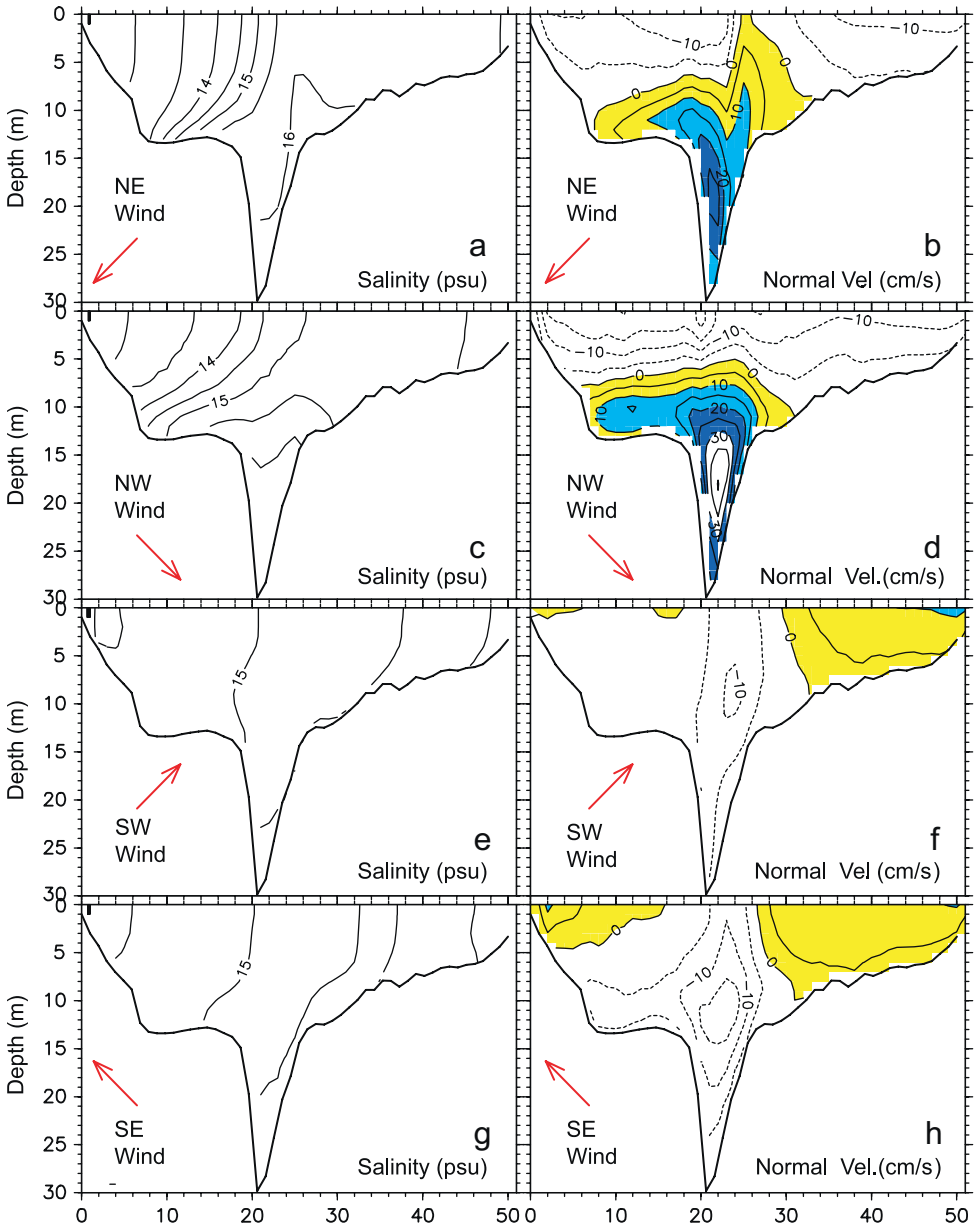

Fig. 7. Vertical distribution of salinity and along-estuary velocity along Section B calculated in cases 1–4. Negative values denote flow toward the bay entrance. The units on the abscissa represent the model grid number.

upper 10 m (Fig. 7a). The wind strengthens the landward inflow, which extends further up to the surface, relative to no-winds, causing transverse shears in the subtidal currents (Fig. 7b). Northwesterly winds change the salinity field the least when compared to the other wind directions (Fig. 7c). On the other hand, these winds strengthen the two-layer circulation (Fig. 7d). Southwesterly winds tend to mix the water column (Fig. 7e) and to reverse the pre-existing estuarine circulation (Fig. 7f). The response consists of downwind flows along the shallow coastal sides and upwind flow along the deep channel of the bay. In other words, southwesterly winds change the pre-existing vertically sheared circulation to a horizontally sheared circulation in the middle and upper bay. Southeasterly winds cause a similar but stronger impact than southwesterly winds on the salinity and subtidal fields (Fig. 7g and h).

At the bay entrance, the effect of winds on the vertical structure of salinity and subtidal currents under bathymetric variations (Fig. 8) seems more complex than in the middle and upper bay (Fig. 7). Northeasterly winds drive coastal waters into the bay and cause near-surface salinity increments, particularly in the northern portion of the bay entrance (Fig. 8a). North of Chesapeake Channel (>12 in the abscissa of Fig. 8a) water-column stratification is rather weak. It is noteworthy that the salinity in the deepest part of Chesapeake Channel decreases relative to the no-wind case (Fig. 3e). This salinity drop illustrates the effects of vertical mixing with the low salinity outflow of the surface layer. The subtidal currents show more transverse variability under northeasterly winds (Fig. 8b) than under no winds (Fig. 3f). The inflow area extends up to the surface while the outflow along the southern coast is maintained. The outflow in the North Channel is slightly weakened by the onshore transport of coastal water.

Northwesterly winds slightly weaken the stratification of the surface layer at the bay entrance (Fig. 8c) relative to the control (no wind) case (Fig. 3e). At the same time, these winds produce a decrease in the salinity below 10 m depth in the Chesapeake

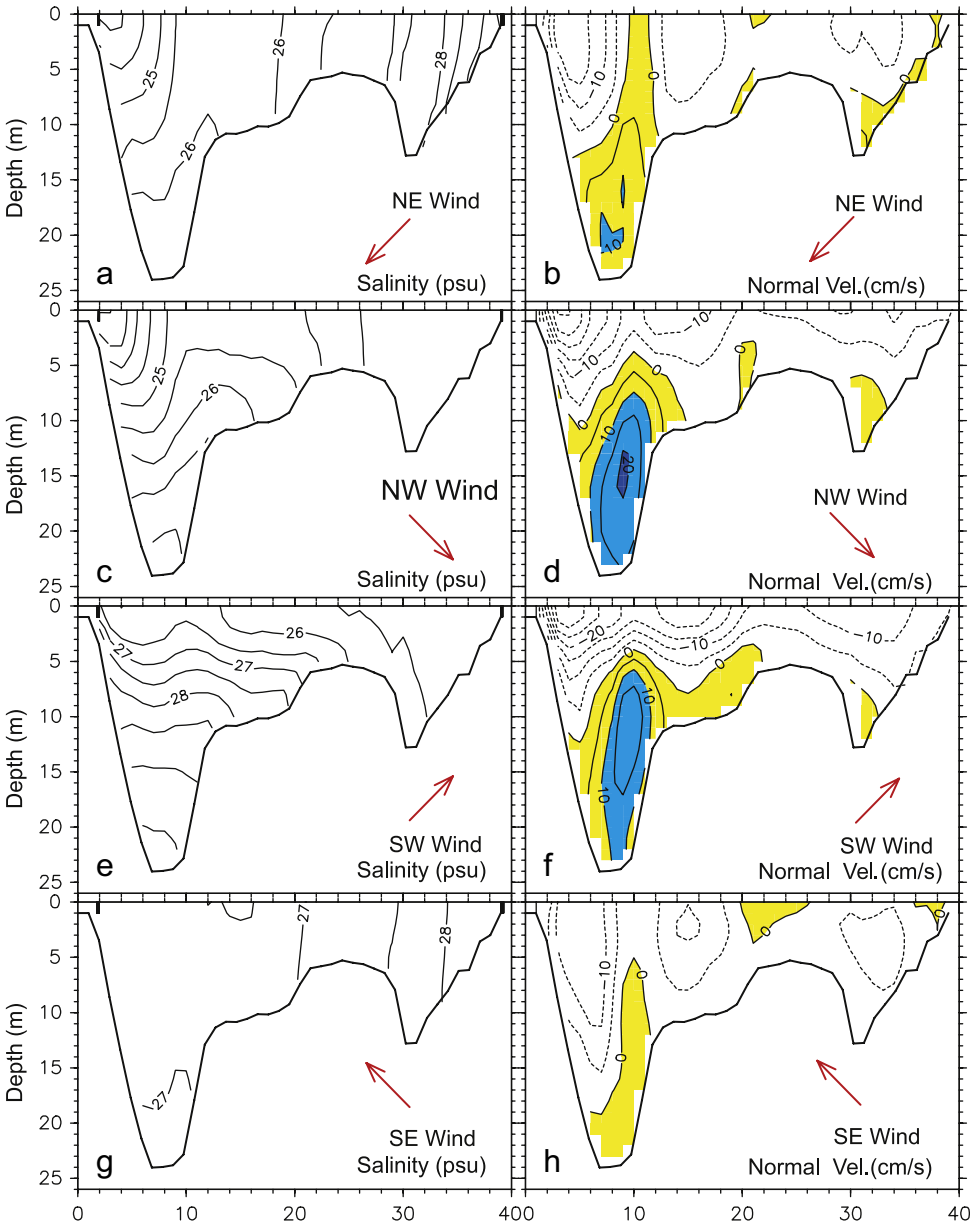

Fig. 8. Vertical distribution of salinity and along-estuary velocity along Section C calculated in cases 1–4. Negative values denote outflow from the bay entrance. The units on the abscissa represent the model grid number.

Channel. They also intensify the outflow in the upper layer and inflow in the lower layer of the Chesapeake Channel (Fig. 8d). The flow in the North Channel does not change appreciably (Fig. 8d).

Southwesterly winds show a marked influence of coastal water on the salinity and subtidal current fields at the bay entrance (Fig. 8e and f). The slope of isohalines is reversed in such a way that the salinity is high in the southern part and low in the northern part (Fig. 8e). This is caused by the wind-induced upwelled waters that appear most prominently off Cape Henry, at the southern end of the transect, and in the deepest part (>10 m depth) of Chesapeake Channel. The two-layer structure of the subtidal currents is intensified by the upwelling-type exchange flow, i.e., downwind flow at the surface and upwind flow underneath (Fig. 8f).

Southeasterly winds drive coastal water with higher salinity into the bay, which can be found in the entire water column at the bay entrance (Fig. 8g). However, volume outflow, and not inflow, dominates the entire section. This is, in fact, caused by a rebounding flux of water inside the bay as explained in Section 3.5.

3.4. *Response of density-driven circulation to sea-level change at bay entrance*

On the basis of observations, Paraso and Valle-Levinson (1996) proposed that sea level at the bay entrance (η_{mouth}) can be predicted from eastward (τ_x) and northward (τ_y) components of wind stresses, as well as barometric pressure (Pa) through the relationship:

$$\eta_{mouth} = 10.58 - [1.06\tau_y + 1.63\tau_x + 10.42 \times 10^{-5}\,\text{Pa}]. \quad (1)$$

Here, the effect of barometric pressure changes is not considered and a value of pressure at equilibrium (1.0153×10^5 Pa) is used. The maximum values of sea-level setup corresponding to

northeasterly, northwesterly, southwesterly, southeasterly winds are 26.9, −5.3, −26.9, and 5.3 cm, respectively. During the period of 3 days of a wind pulse, the sea level is ramped up (or down) to its extreme value in the first 12 h; then it is maintained for 2 days; and then it drops (or increases) to zero in the final 12 h. Such sea-level change was added along the open boundary to examine the response of the pre-existing estuarine circulation.

The imposed sea-level changes in cases 5–8 differ only in their magnitude or in the order of rising or dropping. Hence, the results of one case are easily applicable to the other cases. Only the results of case 5, a sea-level change presumed from a north-easterly wind but without direct wind stress prescription, are presented. A rapid response occurred in the sea level inside the bay as shown in Fig. 9a, which is the difference in sea level along the thalweg of the bay between case 5 and case 0. As expected, the sea level at the bay entrance (~540 in the abscissa of Fig. 9a) rapidly rose to a large value in the first 12 h, kept a high sea level with a maximum value larger than 25 cm in the following 2 days, and finally dropped to zero.

Dynamically, the gradient of sea level rather than sea level itself affects flow fields (Fig. 9b). At the stage of sea-level rising, the sea level is higher at bay entrance than in the upper bay by

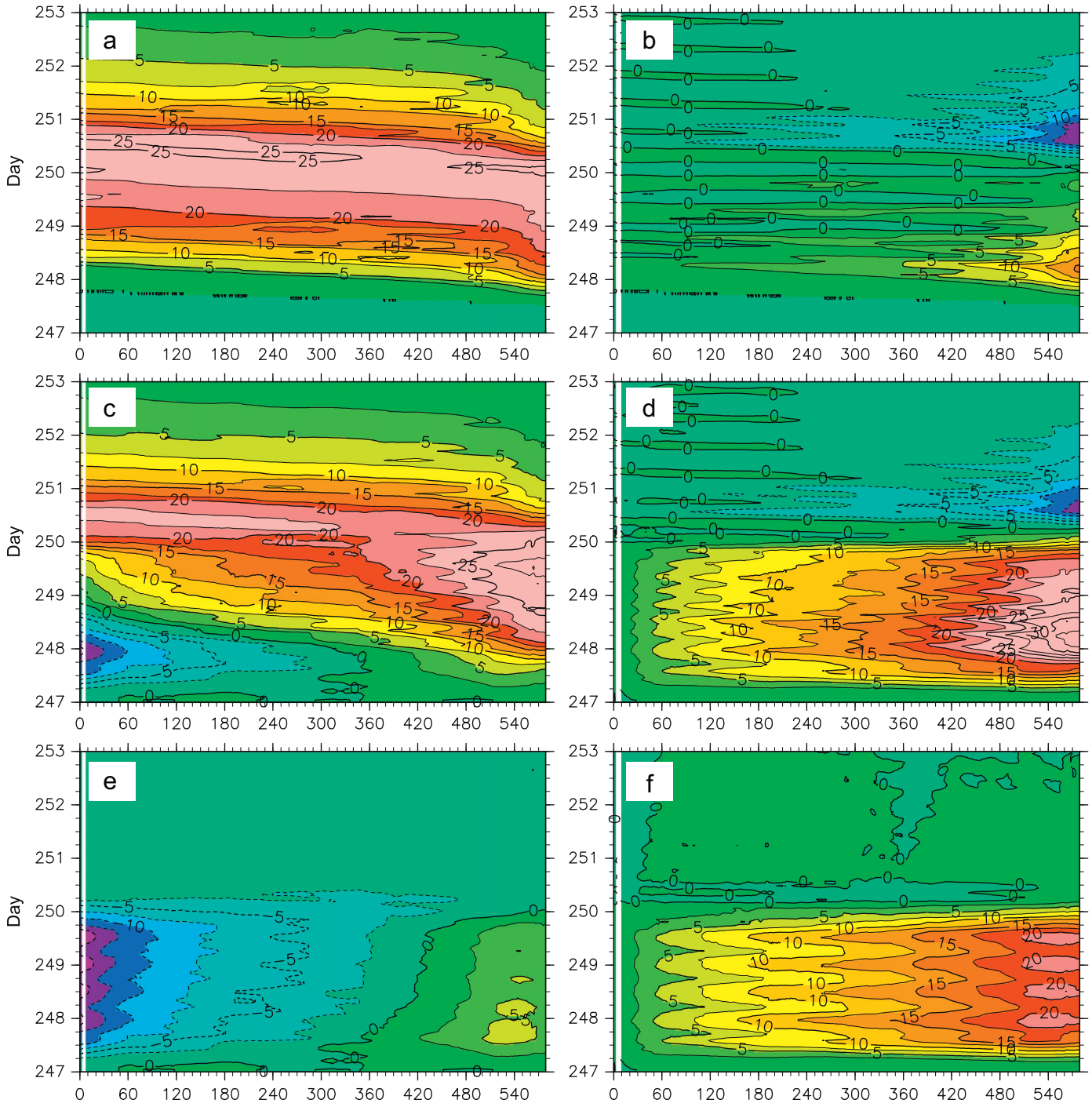

Fig. 9. (a) Anomaly of sea level between case 5 and case 0 along Section A; (b) difference of sea level between each grid point along Section A and the upper bay (grid number = 1) at the same time as in panel (a); (c) the same as (a) but for case 1C and case 0; (d) the same as (b) but for panel (c); (e) the same as (a) but for case 1C and case 5; (f) same as (b) but for panel (e). The number in the contours is in centimeter, the units on the abscissa represent the model grid number along section A.

>10 cm. At the mature stage of the wind, the sea-level difference between bay entrance and upper bay is small (<5 cm). Finally, at the stage of sea-level drop, the situation reverses from the stage of sea-level rising. Spatially, the gradient in sea level caused by remote wind effects is large (maximum of 15 cm) in the lower bay and decreases toward the upper bay.

The inclusion of wind stresses and sea-level setup (as predicted by Eq. (1); case 1C) causes the sea level inside the bay (Fig. 9c) to be less uniform than case 5 (Fig. 9a). A maximum sea-level difference between bay entrance and upper bay reached >30 cm (Fig. 9d). The difference between case 1C (both wind stresses and remote effects) and case 5 (only remote effects) shows that wind stress contributes more to the sea level inside the bay (Fig. 9e) and to the sea-level gradient along the bay (Fig. 9f) than the remote effect. The sign of the sea-level gradient inside the bay caused by wind stress does not depend on the presence (Fig. 9f) or absence (Fig. 4a) of remote effects. Fig. 9 also indicates that wind stress contributes roughly two thirds (>20 cm out of >30 cm) of sea-level difference between the bay entrance and the upper bay. Remote effects contribute the remaining one third. This ratio is kept in the case of southwesterly winds, but drops to a lower value in the cases of northwesterly and southeasterly winds when a lower sea-level change (5.3 cm) was prescribed along the open boundary of model domain.

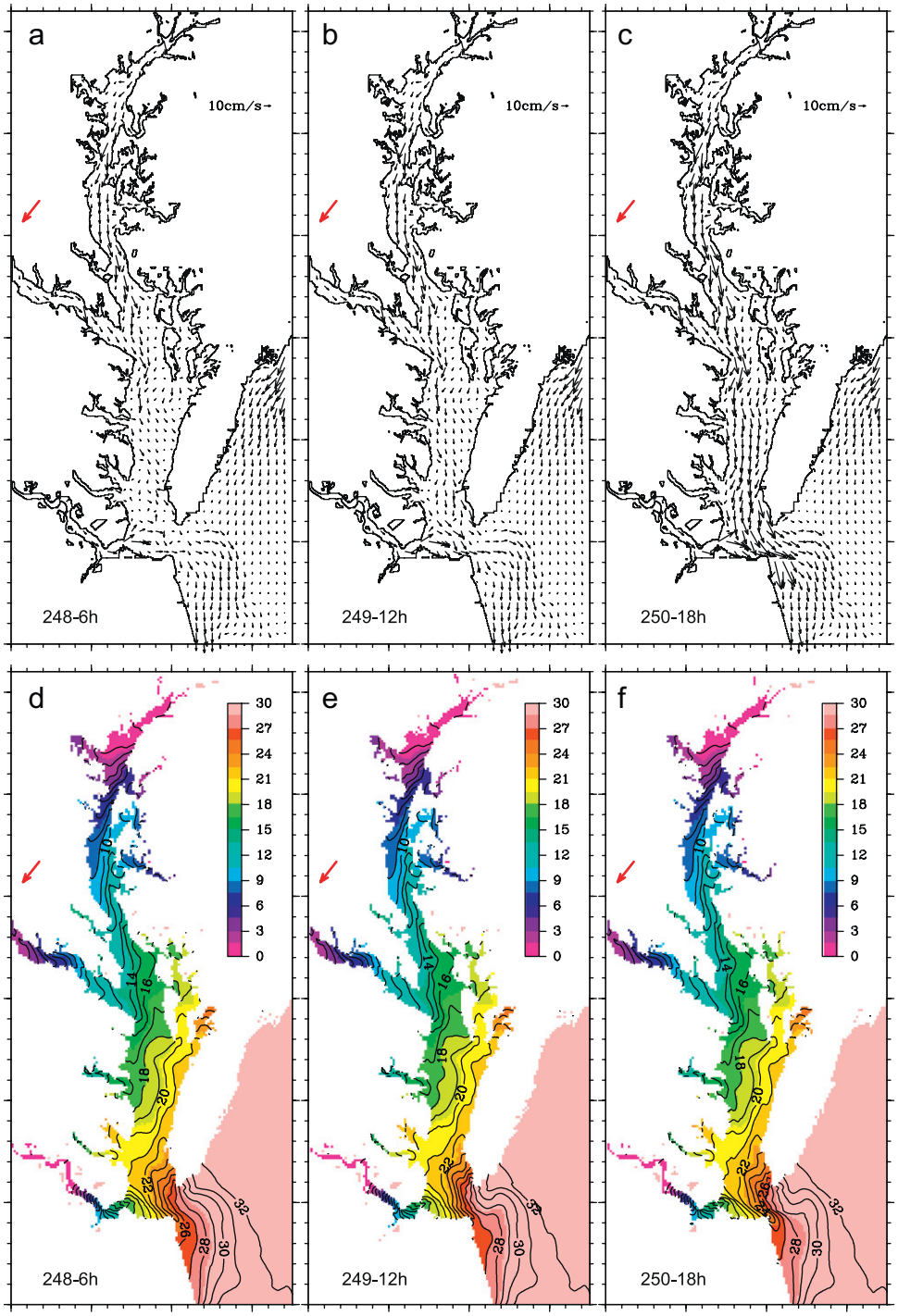

Fig. 10. Horizontal distribution of surface velocity (a–c) and salinity (d–f) calculated for case 5, at 6 h of day 248, 12 h of day 249, and 18 h of day 250.

Fig. 9b shows that remote effects on subtidal flow are strongest at 6 h of day 248 and 18 h of day 250. The seaward pressure gradient at 6 h of day 248 acted against the seaward surface flow and weakened it in the lower bay (Fig. 10a). Analogously, the landward pressure gradient at 18 h of day 250 enhanced the seaward surface flow in the lower bay (Fig. 10c). Between those two days (Fig. 10b), the subtidal flow was very similar to its original state (Fig. 2b), which indicates that the perturbation on subtidal flow due to sea-level change at the bay entrance can vanish in a day or so. The remote effects on surface salinity are generally small and restricted only to near the bay entrance (Fig. 10d–f). Compared with Fig. 2a, the salinity contours at 6 h on day 248 slightly shifted into the bay because of the weakening of seaward surface flow. As the seaward surface flow increased on day 250, the lowest salinity water appeared at southern side of the bay entrance (see position of isohaline 24 in Fig. 10f).

According to the solution by Wong (1994), the current caused by a subtidal sea-level oscillation at the entrance to an estuary is in the same direction throughout the cross-section. Therefore, the surface salinity change near the bay entrance (Fig. 10d–f) is expected to be consistent throughout the entire water column. This is confirmed in Fig. 11 where the surface outflow and the bottom inflow of Fig. 3f were weakened and enhanced, respectively, by the rising of sea level at 6 h of day 248 (Fig. 11d) while salinity increased at the entire transect (Fig. 11a). At 12 h of day 249, salinity kept increasing but the cross-section flow approached the original state (Fig. 3f). At 18 h of day 250, the salinity nearly returned to its initial state (Fig. 3e) while surface outflow and bottom inflow were enhanced and weakened, respectively, by the sea-level drop. The difference in the cross-section flow between the case with remote effects and the control case presents a unidirectional flow through the bay entrance with largest speed above the deepest channel (Fig. 11g–i). All of these features are consistent to the solution given by Wong (1994).

3.5. Volume transport through the bay entrance due to winds

The influence of wind forcing on water exchange in Chesapeake Bay is illustrated by hourly volume transports through the section at the bay entrance (Figs. 12 and 13). The volume transports shown in Figs. 12 and 13 actually represent the difference between cases with winds and the case without winds, i.e., the volume transport due to winds. Volume inflows and outflows respond quickly to the onset of wind forcing on day 247 (Fig. 12) and sea-level change at 12 h of day 247 (Fig. 13a and b), regardless of the wind direction. After the wind stops, it takes ~3 days for the inflow and outflow to return to their original state.

For local wind responses, northeasterly winds produce ~6000–8000 m^3/s of volume outflow in the first 12 h and maintain it for 2 days (Fig. 12a). Inflows develop simultaneously but their magnitude is lower than the outflows. Consequently, net outflows appear on day 249. This response seems to be inconsistent with onshore Ekman transport but is consistent with sea level decreasing in the upper and middle bays (Fig. 4a) as explained with observations by Valle-Levinson et al. (2001). After

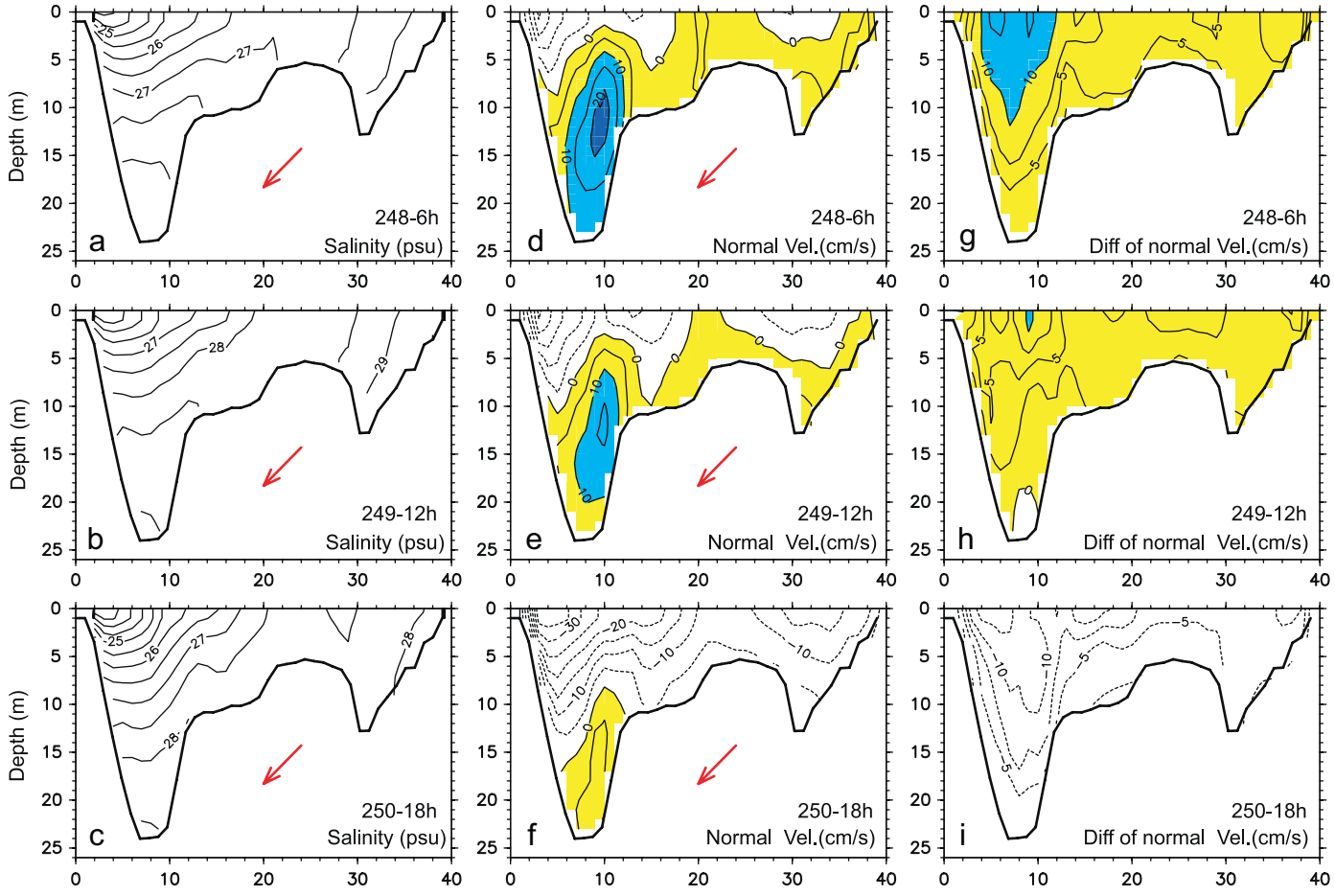

Fig. 11. Vertical distribution of salinity (left panels) and along-estuary velocity (middle panels) calculated by case 5, and difference of along-estuary velocity between case 5 and case 0 (right panels) along Section C, at 6 h of day 248, 12 h of day 249 and 18 h of day 250. Negative values in middle and right panels denote outflow from the bay entrance. The units on the abscissa represent the model grid number.

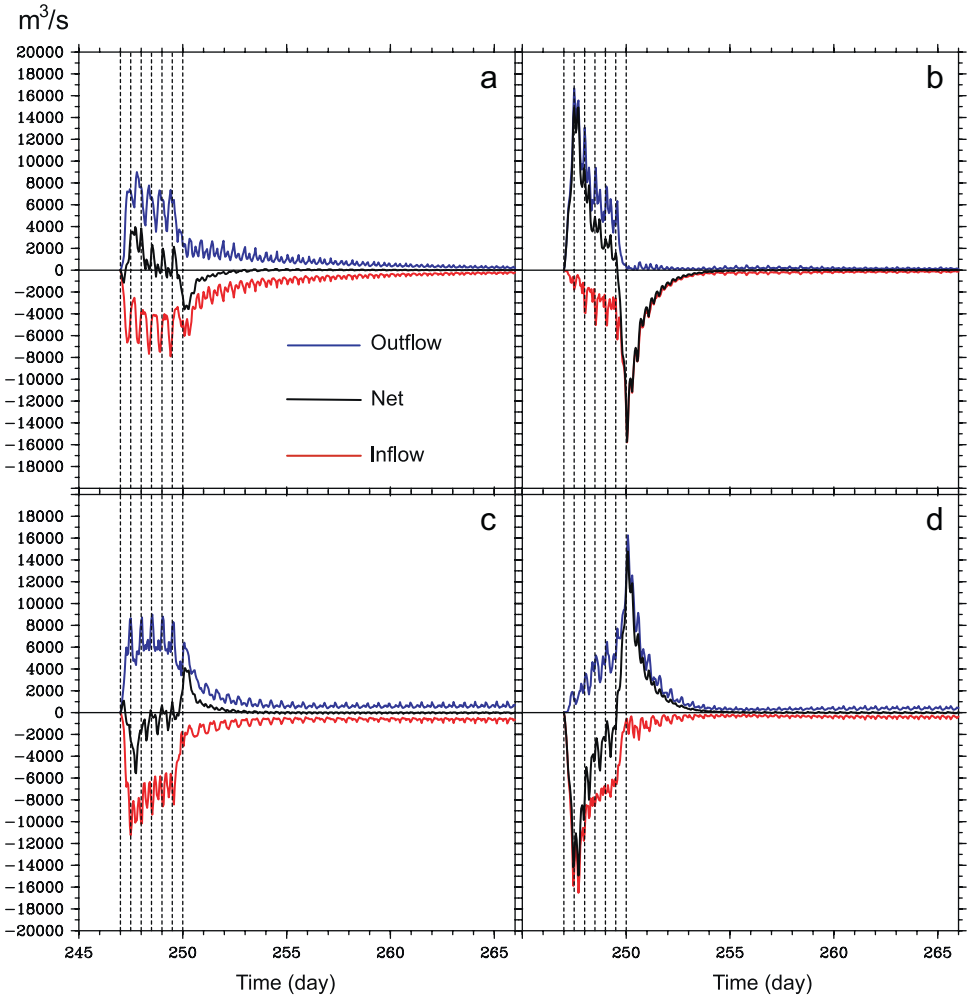

Fig. 12. Temporal variation of volume inflow (negative values), volume outflow (positive values) and net water fluxes through the bay entrance (Section C) between cases 1–4 and case 0.

day 249, the volume in the bay 'bounces back' as inflows exceed outflows. The net volume inflow increases until the wind completely stops and the maximum inflow of 3000 m^3/s is reached. After the wind stops, inflows and outflows decrease simultaneously while net inflows gradually approach zero.

Southwesterly winds produce the opposite response to northeasterly winds (Fig. 12c). The volume inflow in this case reaches ~10,000–12,000 m^3/s in the first 12 h but soon begins to decrease. The inflow exceeds the outflow during most of the wind pulse, being consistent with the sea level increasing in the middle and upper bays (Fig. 4c). After day 249, the outflow exceeds the inflow and results in net outflow that reaches a maximum of 4000 m^3/s at the end of the wind pulse. After that, like in the case of northeasterly winds, both the inflow and outflow decrease and the net flux approaches zero.

Northwesterly (Fig. 12b) and southeasterly (Fig. 12d) winds cause the largest volume fluxes in the cases for local wind effects. This is likely because northwesterly and southeasterly winds act concurrently inside and outside the bay whereas northeasterly and southwesterly winds act in opposing directions inside and outside the bay. For example, northeasterly winds drive water out of the bay within the estuary but at the same time they drive water toward the lower bay from the ocean. Northwesterly winds cause a net outflow of ~16,000 m^3/s in only 1 day. After that the outflow weakens and inflow increases greatly. As the winds stop, the inflow reaches a value of ~16,000 m^3/s and the outflow vanishes. After that the inflow approaches gradually to zero. The response to southeasterly winds is opposite to that of northwesterly winds but the features are similar.

Volume flows indicate that the wind response during transition periods (first and final 12 h) depends on the wind direction (Fig. 12). Northeasterly and southwesterly winds produce bidirectional exchange flows, while northwesterly and southeasterly winds tend to produce only volume inflow or outflow in the entire section. During the periods of mature state of the wind (between the two transition periods), bidirectional flows can be found in all cases. For northeasterly and southwesterly winds, the bidirectional volume flows are maintained throughout the mature wind period. For northwesterly and southeasterly winds, the bidirectional volume exchange develops gradually. The sea-level slopes induced by northwesterly winds (Fig. 4b) cause a gradual development of volume inflow. Similarly, the gradual development of volume outflow in the case of southeasterly winds is caused by the sea-level slopes (set up toward the upper bay, Fig. 4d).

The remote effect due to northeasterly winds produces ~20,000 m^3/s of volume inflow and practically no volume outflow in the first 18 h (Fig. 13a). The volume inflow reaches its maximum value at 6 h on day 248, when the seaward sea-level gradient at the bay entrance is greatest (Fig. 9b). After the maximum volume inflow, the transport starts to drop gradually with the reduction of the seaward sea-level gradient at the bay entrance (Fig. 9b). The

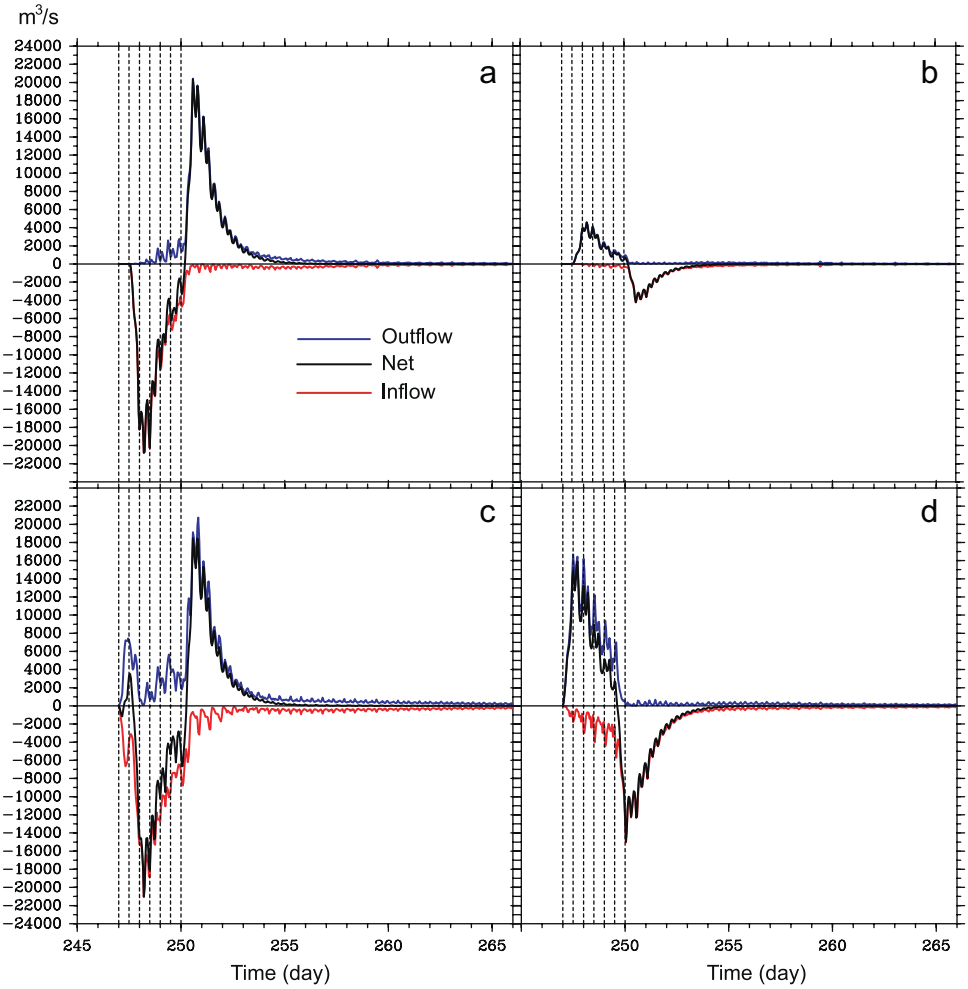

Fig. 13. Same as Fig. 12 but for those between case 5 and case 0 (a), between case 6 and case 0 (b), between case 1C and case 0 (c), and between case 2C and case 0 (d).

volume inflow becomes zero as the sea level at bay entrance reaches its maximum at 0 h of day 250, corresponding to nearly zero sea-level gradient (Fig. 9a). Subsequently, volume outflow appeared along with landward sea-level gradient at the bay entrance, reaching ~20,000 m^3/s at 18 h of day 250, and then gradually drops to zero (Fig. 13a).

The remote effects due to northwesterly winds cause a volume outflow first and then a volume inflow (Fig. 13b). The maximum volume fluxes (~4000 m^3/s) are one-fifth of those produced by northeasterly winds. This is because the sea-level change prescribed at the open boundary is 5.3 cm for northwesterly winds compared to 26.9 cm for northeasterly winds.

The analytical solution of Wong (1994) suggests that the local response to winds consists of bidirectional currents while the remote effect causes unidirectional currents. Following that solution, volume inflows and outflows are of the same order of magnitude and both of them are larger than the net volume flow if the local effect dominates. If the remote effect dominates, either the volume inflow or the outflow is much larger than the other and is comparable to the net flux. In the middle and upper bay, the lateral distribution of current caused by local wind stresses (Fig. 7) and the landward reduction of response in flow fields to sea-level change prescribed at the open boundary of the model domain (Fig. 10) suggest that the local effect of wind dominates. At the bay entrance, the remote effect given by a sea-level change at the open boundary produces only volume inflows or outflows (Fig. 13a and b), and therefore dominates the volume fluxes there.

In his estimate for remote effects of wind, Wong (1994) used sea-level setup or set-down at a constant rate as the only forcing. This formulation suggests that the remote effects are proportional to the rate of change of subtidal sea-level change at the bay entrance. Therefore, the relation between volume inflow or outflow and the rate of sea-level rise or drop at the open boundary (Fig. 13a and b) is actually controlled by the rate of sea-level rise or drop at the bay entrance. In the calculations presented here, all wind events span the same period and therefore the rate of sea-level change is proportional to the values given in Table 1. In a limiting case such as at steady state, the remote effect approaches zero (Wong and Valle-Levinson, 2002). This also occurs in the model results as the sea level at the bay entrance reaches the highest level while the landward sea-level gradient disappears (Fig. 9a and b).

The combination of local and remote wind effects suggests that either of these two dominate at different periods of a wind pulse. For northeasterly winds (Fig. 13c), because of the lag between sea-level change and local winds (Paraso and Valle-Levinson, 1996), the initial response is the appearance of bidirectional volume flows due to local effects. The remote effects gradually increase and soon overcome the local effects. At the end stage of a northeasterly wind pulse, the local effects dominate again. As the wind stresses completely stop and the sea level at the bay entrance drops, the remote effects become dominant again. For northwesterly winds (Fig. 13d), except for the end stage when bidirectional volume flows overcome the net volume transport,

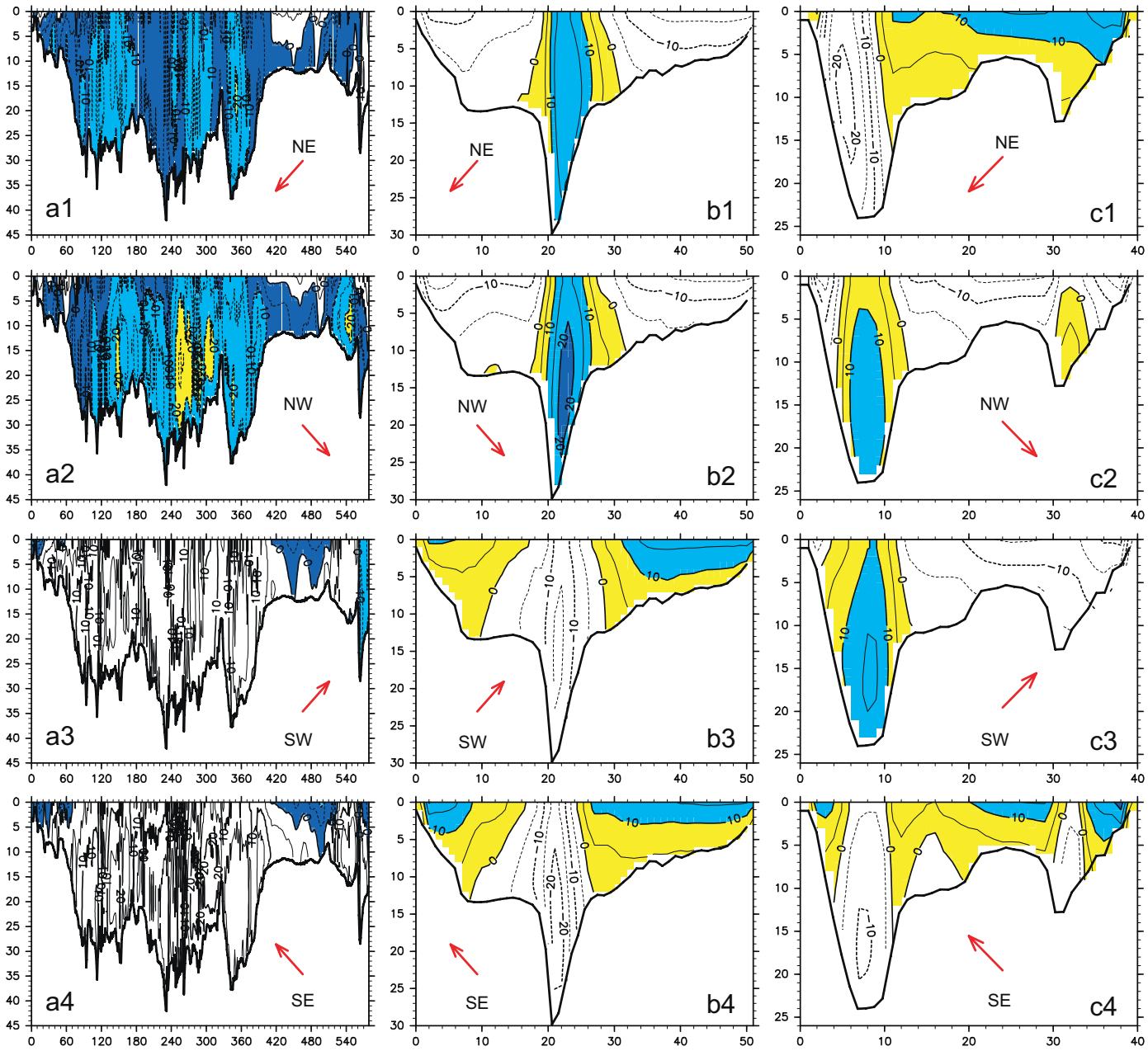

Fig. 14. Vertical distribution of along-estuary velocity, parallel to Section A (left panels), normal to Section B (middle panels) and normal to Section C (right panels) calculated by the winds given in cases 1–4 but with a constant density throughout the model domain. The units on the abscissa represent the model grid number.

unidirectional volume transports are dominant role of remote effects under northwesterly winds appears even in the calculation for local wind forcing (Fig. 12b). This is evident during the transition periods, as the wind stress increases in the first 12 h or decreases in the last 12 h.

4. Discussion

4.1. Wind-induced currents under homogeneous conditions

The linear superposition of wind-induced currents under homogeneous conditions and estuarine currents has been used in several studies (e.g., Hansen and Rattray, 1965; Wong, 1994; Geyer, 1997). Following this approach, wind-induced currents were obtained under homogeneous conditions (constant water density) throughout the bay and without tide. These calculations are denoted as case 1H to case 4H, hereafter. It should be noted that the wind-induced currents under homogenous condition in an idealized bathymetry with or without Earth's rotation have been studied extensively (e.g., Csanady, 1982; Hunter and Hearn, 1987; Hearn et al., 1987; Wong, 1994; Friedrichs and Hamrick, 1996; Mathieu et al., 2002; Winant, 2004; Sanay and Valle-Levinson, 2005).

Under homogeneous conditions, the wind-induced currents inside the bay are affected by bathymetry. Bathymetric effects on flows are best illustrated in cross-sections (Fig. 14). Along the thalweg of the bay, the currents are persistently upwind (Fig. 14a1–a4). This feature is consistent with analytical solutions (e.g., Wong, 1994; Winant, 2004) in the sense that the current in the deep portions of a transverse section is upwind and that over the shallow portions is downwind. In addition to this transverse

structure, analytical solutions also indicate that the upwind current is bottom-intensified while the downwind current is surface-intensified. All these features can be observed at the section in middle bay (Fig. 14b1–b4) and at the bay entrance in the cases of northwesterly and southeasterly winds (Fig. 14c2 and c4). In the cases of northeasterly and southwesterly winds, the water at the bay entrance responds not only to the wind stress inside the bay but also to the onshore or offshore transport outside the bay. The vertical structure shows that the inflow or outflow in the northern part of bay entrance (>10 in the abscissa of Fig. 14c1 and c3) is not limited to the surface layer but occurs in the entire water column. At the same time, an opposite flow develops in the entire water column in Chesapeake Channel, resulting in appreciable lateral variability in this section (Fig. 14c1 and c3).

4.2. *Effects of density gradients on the response of the bay to winds*

The differences in the subtidal currents between cases 1–4 and case 0 represent the response of estuarine circulation to winds (Fig. 15). Comparison of such differences with the wind-induced currents in the homogeneous condition (Fig. 14) clearly illustrates the influence of density gradients (both horizontal and vertical gradients) on the response of the subtidal flow to winds. The density gradients cause the wind-induced currents to show more vertical structure (Fig. 15) than under homogeneous conditions. For northwesterly and southeasterly winds, the currents along the thalweg are downwind at the surface and upwind underneath (Fig. 15a2 and a4). Under northeasterly and southwesterly winds, the flow shows a two-layer or even three-layer structure (Fig. 15a1 and a3).

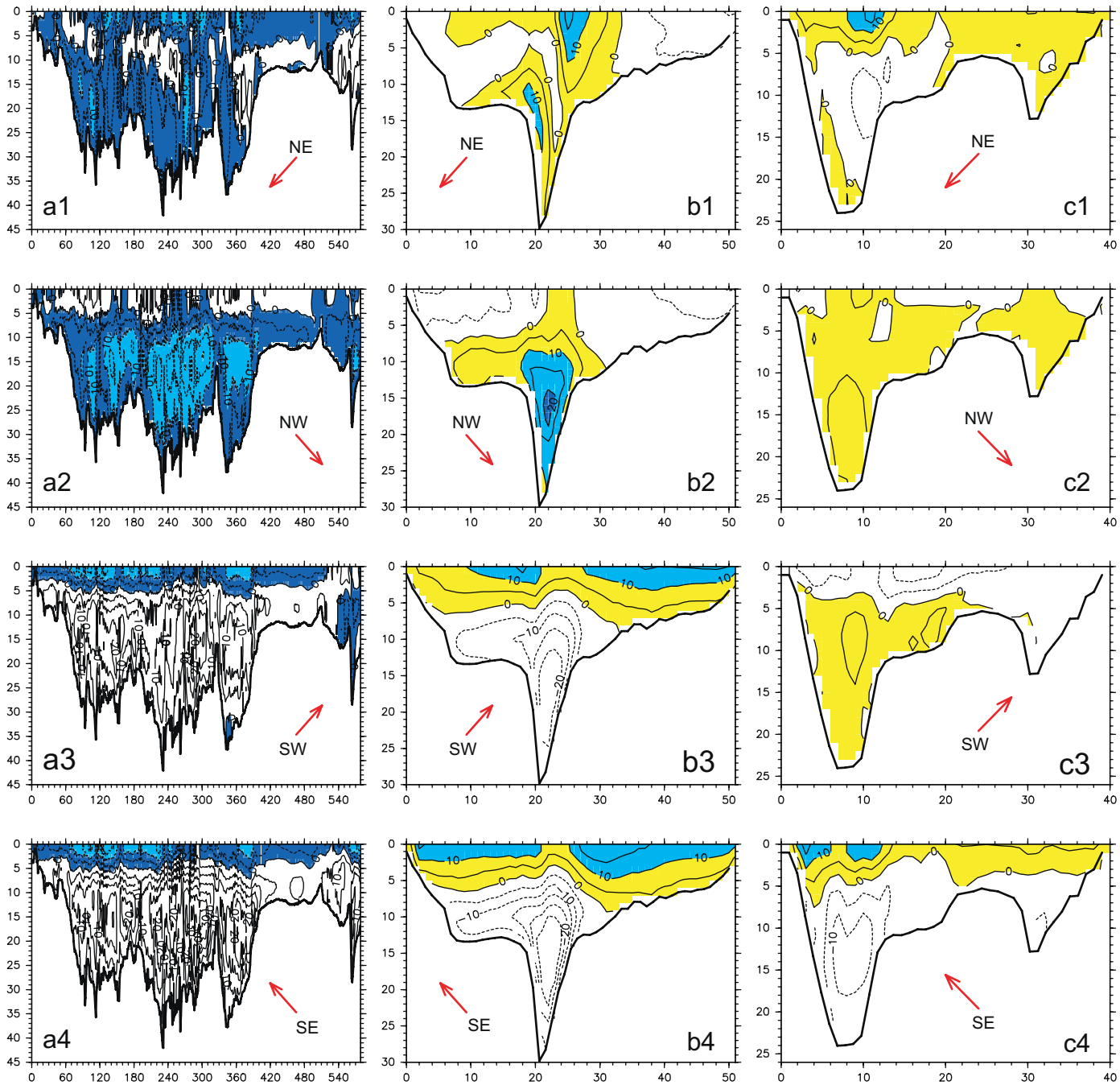

Fig. 15. Same as Fig. 14 but for the difference between cases 1–4 and case 0.

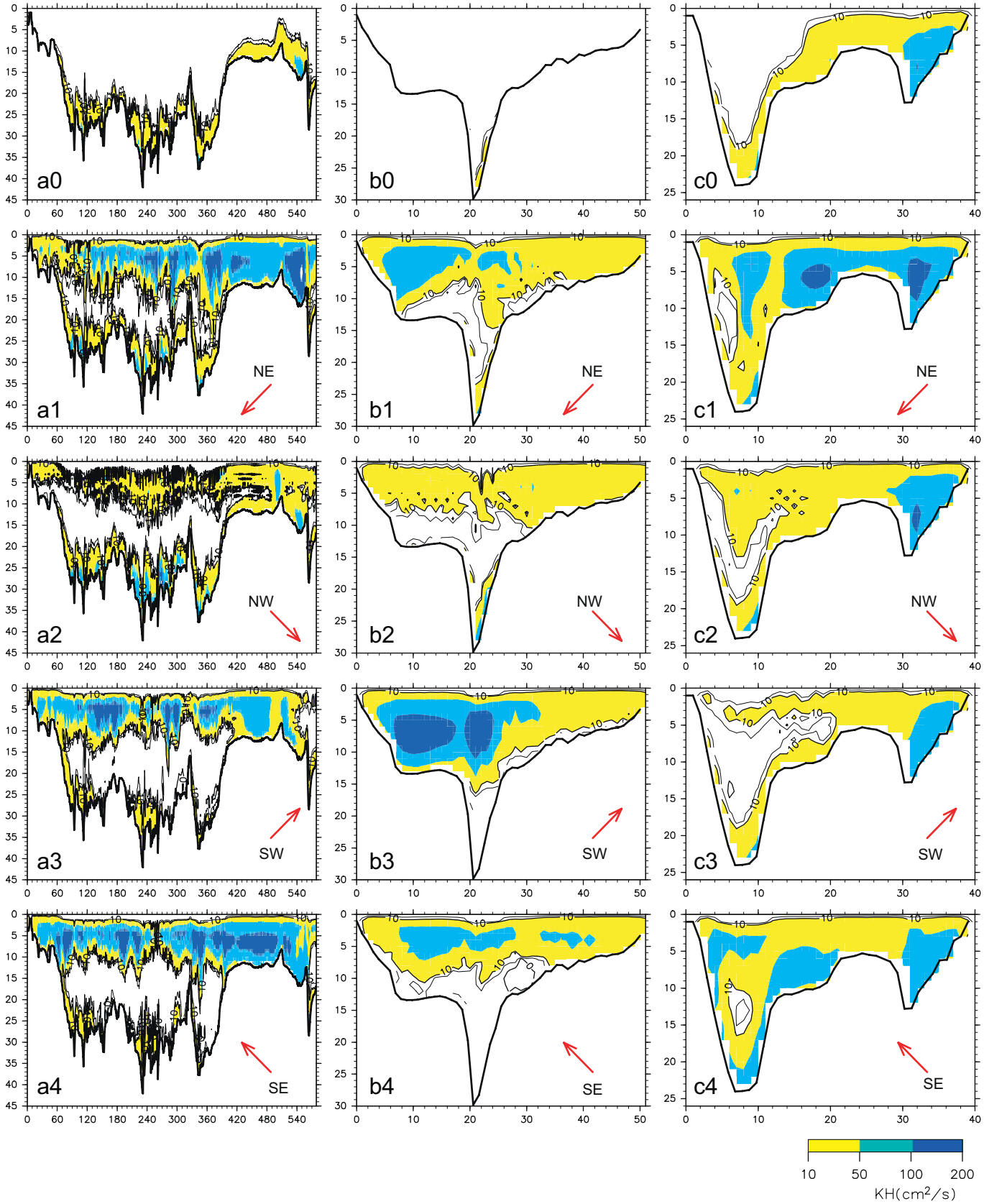

Fig. 16. Distribution of eddy viscosity along Section A (left panels), along Section B (middle panels) and along Section C (right panels) calculated for case 0 (top panels) and cases 1–4.

The vertical structure of the wind-induced currents in the presence of stratification is also illustrated in the mid-bay section (Fig. 15b1–b4). For northeasterly winds, a relatively weak (<5 cm/s) down-estuary current on the shoals separates a stronger (>10 cm/s) up-estuary current in the channel (Fig. 15b1). Also, a three-layer structure develops over the western shoal. Northwesterly winds produce a similar flow pattern as for the homogeneous condition but the upwind surface current is weaker (Fig. 15b2). Southwesterly and southeasterly winds produce a well-developed two-layer structure of wind-induced currents, which is downwind at the surface and upwind underneath (Fig. 15b3 and b4).

In the presence of stratification, the wind-driven flow is confined to a surface layer at the bay mouth (Fig. 15c1 and c3). Northeasterly winds drive water into the bay within the upper 5 m, while southwesterly winds drive water out of the bay. In the Chesapeake Channel, these winds produce bidirectional exchange flows that differ from the unidirectional flows arising under homogeneous conditions (Fig. 14c1 and c3). Northwesterly and southeasterly winds also produce a two-layer structure that differs from the one-layer response under homogeneous conditions.

As shown above, wind-driven currents over laterally variable bathymetry are significantly different from stratified to homogeneous conditions. Wind-induced currents under stratified conditions tend to be vertically sheared while those in homogeneous conditions tend to be horizontally sheared. This is consistent with the findings of Lentz (2001) on the continental

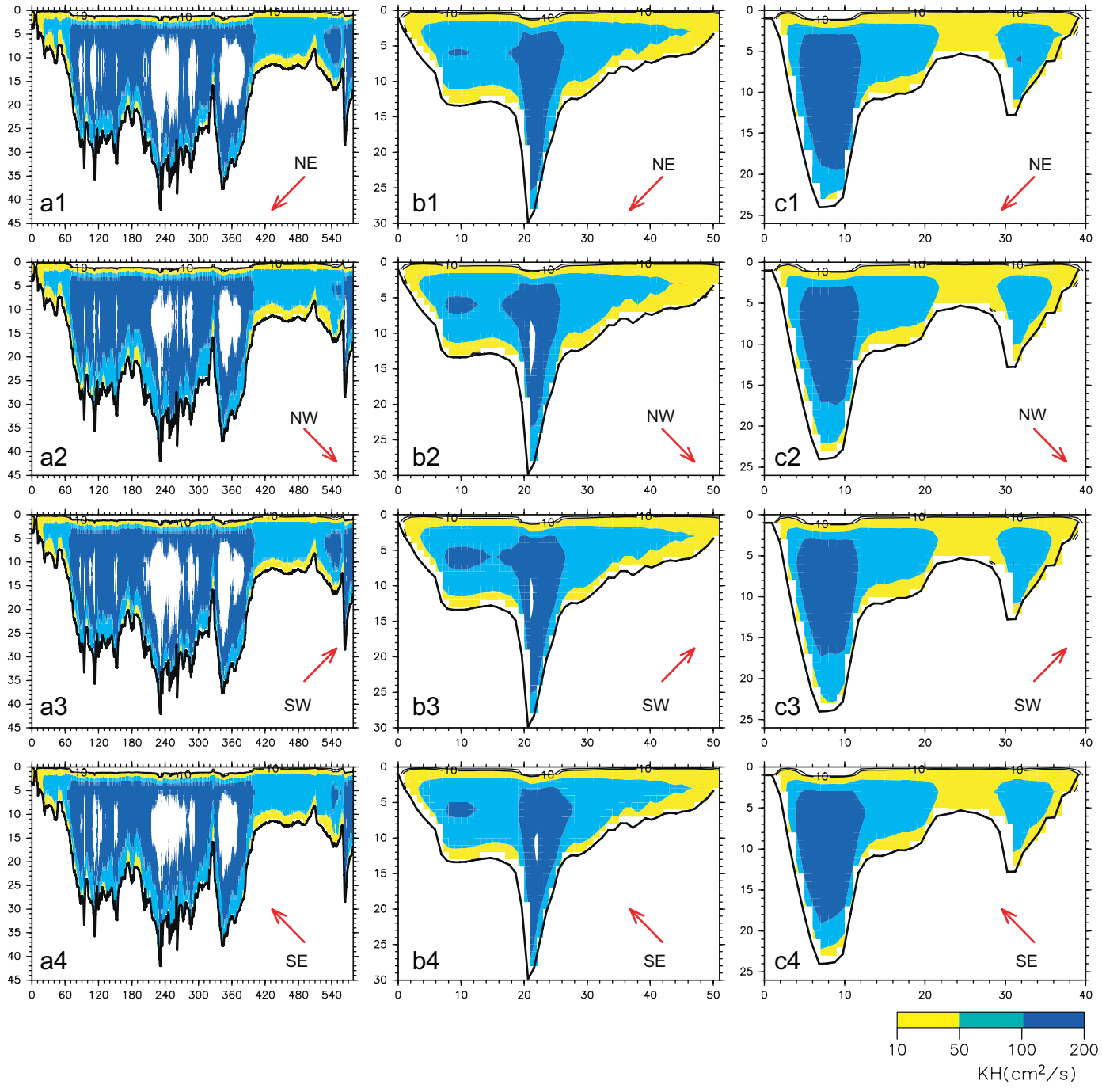

Fig. 17. Same as Fig. 16 but for cases 1H–4H, in which the density is constant throughout the model domain.

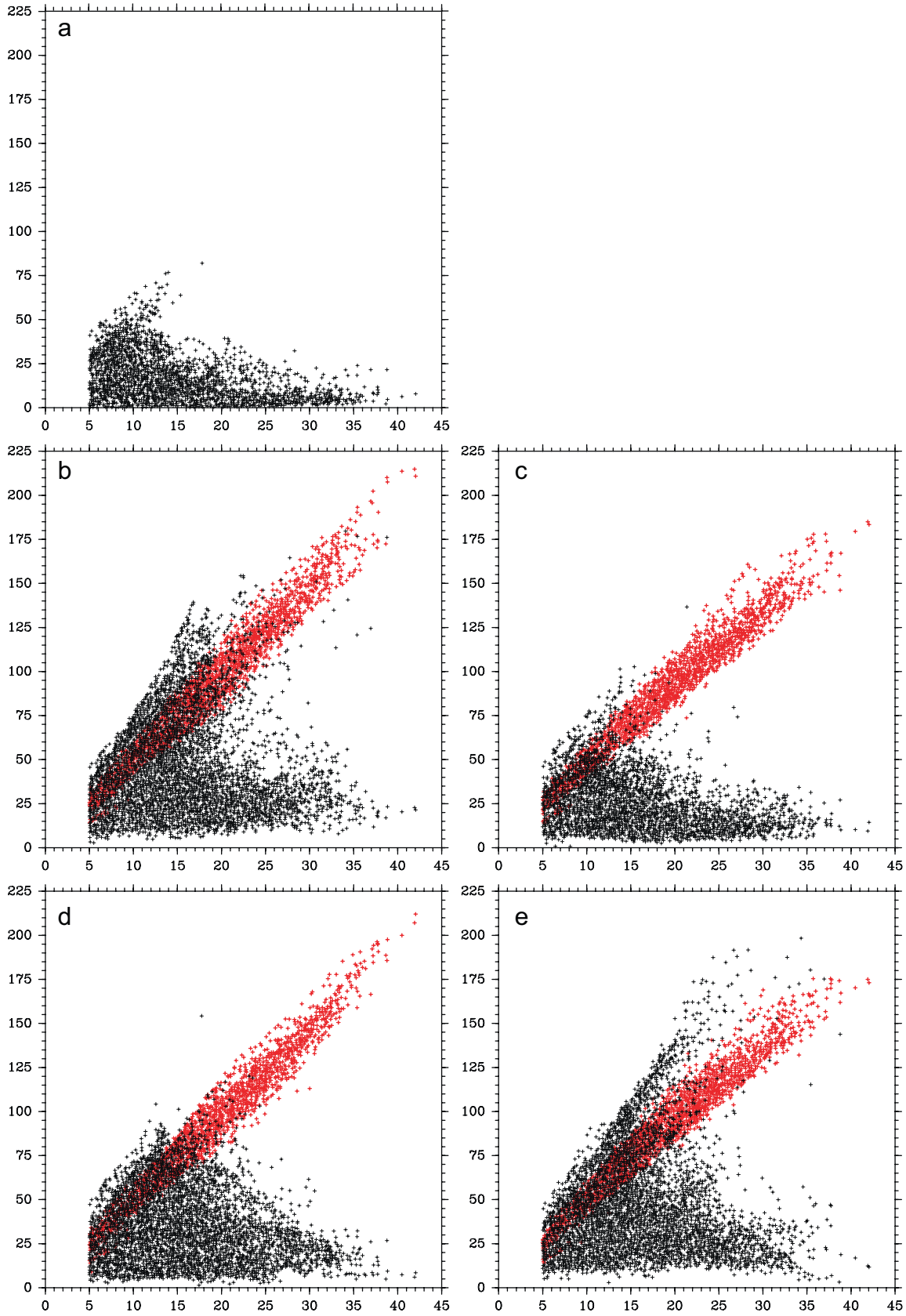

Fig. 18. Vertically averaged vertical eddy viscosity coefficients (ordinate, in units of cm^2/s^{-1}) versus water depth (abscissa, in units of meter) in case 0 (top panel), cases 1–4 (black symbols in the middle and bottom panels), and cases 1H–4H (red symbols in the middle and bottom panels). *Note*: (a) No Wind, (b) NE Wind, (c) NW Wind, (d) SW Wind and (e) SE Wind.

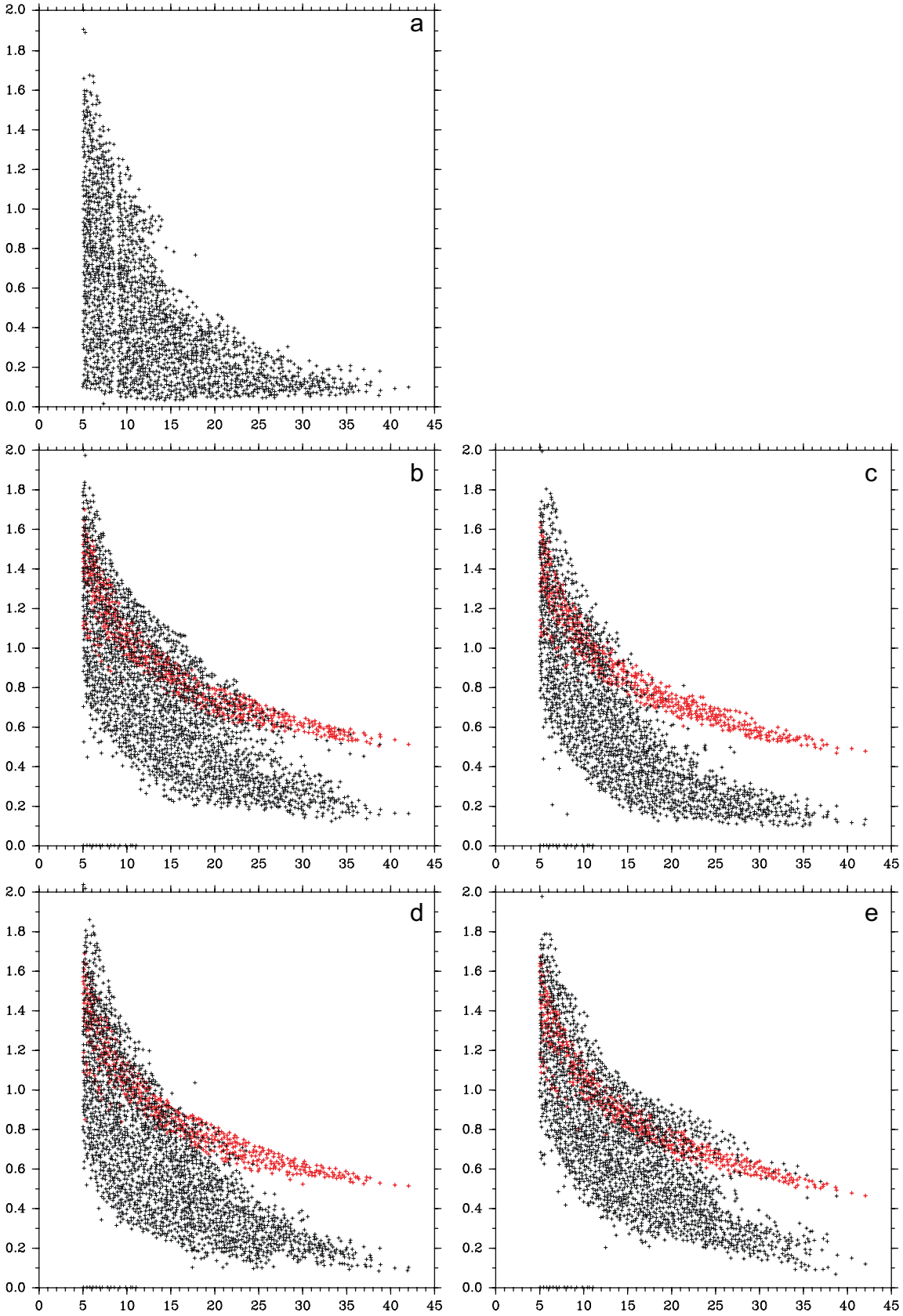

Fig. 19. Ratio of Ekman depth ($\sqrt{2K_v/f}$, K_v = vertically averaged eddy viscosity, f = Coriolis parameter) to water depth (ordinate) versus water depth (abscissa, in units of meter) for case 0 (top panel), cases 1–4 (black symbols in the middle and bottom panels), and cases 1H–4H (red symbols in the middle and bottom panels). *Note*: (a) No Wind, (b) NE Wind, (c) NW Wind, (d) SW Wind and (e) SE Wind.

shelf. Two causes should be responsible for this different response in the model experiments. The first cause is the change in the density field, namely the horizontal density gradient, caused by winds. A change in horizontal density gradients would modify the pre-existing estuarine circulation. However, the horizontal distribution of salinity (Fig. 5) suggests that wind-induced modifications are localized but are small at the scales of the entire bay and cannot explain the different current structures shown in Figs. 14 and 15. The second cause is the wind-induced structure of the turbulence field. As shown by Kasai et al. (2000) and Valle-Levinson et al. (2003), increased internal friction tends to enhance the transverse structure of the subtidal currents. Examination of the vertical eddy viscosity coefficients for cases 0–5 and 1H–4H illustrates the different structure of the wind-induced currents for the homogeneous and stratified conditions driven by the same wind condition.

4.3. Wind-induced mixing and Ekman depth

In the cases that included wind forcing, the vertical eddy viscosity coefficient calculated by the Mellor-Yamada turbulent closure model increases significantly at mid-depth (Fig. 16). Without winds (Fig. 16a0–c0), the eddy viscosity coefficients are large only near the bottom, particularly at the bay entrance, resulting from tidal currents (Guo and Valle-Levinson, 2007). As winds are imposed, the eddy viscosity coefficients increase significantly at mid-depth and maximum values reach 10–200 cm^2/s. The vertical eddy viscosities increase the least in the case of northwesterly winds, which cause the least destratification (Figs. 7 and 8). Interestingly, without stratification, the vertical eddy viscosities depend little on the wind direction (Fig. 17). The eddy viscosities are larger in the homogeneous cases than in the corresponding stratified cases and the areas with coefficients $>100\,cm^2/s$ are widespread. Because the vertical profile of eddy viscosity in neutral conditions (destratified, no buoyancy forcing) from the Mellor-Yamada level 2.5 turbulence closure is parabolic (see Fig. 6 in Lentz, 2001), the largest values appear at mid-depth and over the deepest places of a cross-section. When plotting the vertically averaged eddy viscosity versus the water depth for the grids inside the bay, a quasi-linear relation is obtained (red symbols in Fig. 18). This is consistent with the depth-dependent formulation used in other studies (e.g., Friedrichs and Hamrick, 1996).

A linear relationship between eddy viscosity and water depth does not hold, however, in the presence of stratification, regardless of the presence or absence of winds (Fig. 18). In the case of no wind, an eddy viscosity near $0\,cm^2/s$ can be found for all depths. The tidal currents around the bay mouth contribute to the relatively large values for depths of 5–20 m. The prescription of winds causes an increase of the minimum eddy viscosity to 5–10 cm^2/s and also a significant increase for all depths. It is noteworthy that the maximum eddy viscosities for depths between 5 and 20 m exceed those for the homogeneous cases, most clearly for the cases of northeasterly and southeasterly winds.

The ratio of Ekman layer depth ($\sqrt{2K_v/f}$, K_v = vertically averaged eddy viscosity, f = Coriolis parameter) versus the water depth is plotted for cases 0–4 and 1H–4H in Fig. 19. The ratio of 0.6–1.6 in the homogeneous cases (red symbols in Fig. 19) indicates that bathymetry molds the wind-driven current inside the bay. This is because the Ekman layer occupies all or most of the water column. The presence of stratification reduces the Ekman layer depth and in the deep channel (20–40 m) the ratio becomes typically <0.2 (no wind in Fig. 19). Wind forcing increases the ratio (typically >0.2) for all depths and also the minimum ratio over the shallow places increases markedly. The presence of stratification limits the Ekman layer depth and reduces bathymetric effects. For all depths, the ratio decreases relative to homogeneous conditions. Therefore, the wind-induced variations in the flow field tend to have a vertically sheared two-layer structure (Fig. 15). In the homogeneous cases, the Ekman layer depth reaches the same order as the water depth (Fig. 19) and therefore bathymetric effects appear clearly in the laterally sheared wind-driven flow (Fig. 14).

5. Summary

In this study, the response of the density-driven (estuarine) circulation in Chesapeake Bay to winds from four directions and the induced sea-level changes outside the bay is investigated. In general, northeasterly and northwesterly winds enhance the estuarine circulation inside the bay while southeasterly and southwesterly winds weaken it. In the lower bay, the response is different because the wind-driven onshore transport (for northeasterly winds) or offshore transport (for southwesterly winds) outside the bay competes with the downwind transport within the bay. Remote wind effects dominate volume transports through the bay entrance. However, the local effect is the main responsible for sea-level slopes that drive the flows and salinity fields in most of the bay under stratified conditions.

The response of the bay to wind depends on whether the water column is stratified or not. The absence of stratification allows the development of Ekman layers that attain depths of the same order as the water depth. Consequently, bathymetric effects become prominent on the flow structure and the wind-induced flow inside the bay is laterally sheared because of the appearance of downwind flow over the flanks and upwind flow in the channel. In the presence of stratification, Ekman layers attain shallower depths than in the absence of stratification. Therefore, the wind-induced currents are less influenced by bathymetry and become vertically, rather than laterally, sheared with downwind flow at the surface and upwind flow underneath.

The change of orientation of the Chesapeake Bay axis in the lower bay is crucial to cause different responses to winds from the upper-mid bay to the lower bay. It should be noted that the stratification that develops in the control case is produced by the annual river discharge and it is usually weaker than the real springtime situation. The imposed winds are also idealized. In the future, the influence of variations in river discharge and the temporal and spatial variations in the wind field need to be addressed.

Acknowledgments

X. Guo acknowledges support by Grant-in-Aid for Global COE Program from the Ministry of Education, Culture, Sports, Science, and Technology, Japan (MEXT); and the Japan Society for the Promotion of Science (JSPS). A.V.L. acknowledges support from NSF Projects 0551923 and 0603540.

References

Beardsley, R.C., Boicourt, W.C., 1981. On estuarine and continental shelf circulation in the Middle Atlantic Bight. In: Warren, B.A., Wunsch, C. (Eds.), Evolution of Physical Oceanography. The MIT Press, pp. 198–233.

Chao, S.-Y., 1988. Wind-driven motion of estuarine plumes. Journal of Physical Oceanography 18, 1144–1166.

Csanady, G.T., 1982. Circulation in the Coastal Ocean. D. Reidel, 279pp.

Elliott, A.J., 1978. Observations of the meteorologically induced circulation in the Potomac estuary. Estuarine, Coastal and Shelf Science 6, 285–300.

Epifanio, C.E., Garvine, R.W., 2001. Larval transport on the Atlantic continental shelf of North America: a review. Estuarine, Coastal and Shelf Science 52, 51–77.
Friedrichs, C.T., Hamrick, J.M., 1996. Effects of channel geometry on cross sectional variations in along channel velocity in partially stratified estuaries. In: Aubrey, D. (Ed.), Buoyancy Effects on Coastal and Estuarine Dynamics, Coastal and Estuarine Studies, 53. American Geophysical Union, pp. 283–300.
Geyer, W.R., 1997. Influence of wind on dynamics and flushing of shallow estuaries. Estuarine, Coastal and Shelf Science 44, 713–722.
Goodrich, D.M., Boicourt, W.C., Hamilton, P., Pritchard, D.W., 1987. Wind-induced destratification in Chesapeake Bay. Journal of Physical Oceanography 17, 2232–2240.
Guo, X., Valle-Levinson, A., 2007. Tidal effects on estuarine circulation and outflow plume in the Chesapeake Bay. Continental Shelf Research 27, 20–42.
Fong, D.A., Geyer, W.R., 2001. Response of a river plume during an upwelling favorable wind event. Journal of Geophysical Research 106, 1067–1084.
Hanawa, K., Mitsudera, H., 1985. On daily average of oceanographic data. Coastal Oceanographic Bulletin 23, 79–87 (in Japanese).
Hansen, D.V., Rattray Jr., M., 1965. Gravitational circulation in straits and estuaries. Journal of Marine Research 23, 104–122.
Hargis, W.J., 1980. A Benchmark Multi-Disciplinary Study of the Interaction Between the Chesapeake Bay and Adjacent Waters. Chesapeake Bay Plume Study Superflux 1980. NASA Conference Publication 2188, Williamsburg, VA, pp. 1–14.
Hearn, C.J., Hunter, J.R., Heron, M., 1987. The effects of a deep channel on the wind-induced flushing of a shallow bay or harbor. Journal of Geophysical Research 92, 3913–3924.
Hunter, J.R., Hearn, C.J., 1987. Lateral and vertical variations in the wind-driven circulation in long, shallow lakes. Journal of Geophysical Research 92, 13106–13114.
Kasai, A., Hill, A.E., Fujiwara, T., Simpson, J.H., 2000. Effect of the earth's rotation on the circulation in regions of freshwater influence. Journal of Geophysical Research 105, 16961–16969.
Lentz, S.J., 2001. The influence of stratification on the wind-driven cross-shelf circulation over the North Carolina shelf. Journal of Physical Oceanography 31, 2749–2760.
Mathieu, P.P., Deleersnijder, E., Cushman-Roisin, B., Beckers, J.M., Bolding, K., 2002. The role of topography in small well mixed bays, with application to the lagoon of Mururoa. Continental Shelf Research 22, 1379–1395.
Mellor, G.L., 2004. Users guide for a three-dimensional, primitive equation, numerical ocean model, 53pp. Program in Atmosphere and Ocean. Science, Princeton University.
Paraso, M.C., Valle-Levinson, A., 1996. Meteorological influences on sea level and water temperature in the lower Chesapeake Bay: 1992. Estuaries 19, 548–561.
Salas-Monreal, D., Valle-Levinson, A., 2008. Sea level slopes and volume fluxes produced by atmospheric forcing in estuaries: Chesapeake Bay case study. Journal of Coastal Research 24, 208–217.
Sanay, R., Valle-Levinson, A., 2005. Wind-induced circulation in semienclosed homogeneous, rotating basins. Journal of Physical Oceanography 35, 2520–2531.
Seitz, R.C., 1971. Temperature and salinity distributions in vertical sections along the longitudinal axis and across the entrance of the Chesapeake Bay (April 1968 to March 1969). Chesapeake Bay Institute, The Johns Hopkins University, 99pp.
Valle-Levinson, A., Li, C., Royer, T.C., Atkinson, L.P., 1998. Flow patterns at the Chesapeake Bay entrance. Continental Shelf Research 18, 1157–1177.
Valle-Levinson, A., Wong, K.-C., Bosley, K.T., 2001. Observations of the wind-induced exchange at the entrance to Chesapeake Bay. Journal of Marine Research 59, 391–416.
Valle-Levinson, A., Wong, K.-C., Bosley, K.T., 2002. Response of the lower Chesapeake Bay to forcing from Hurricane Floyd. Continental Shelf Research 22, 1715–1729.
Valle-Levinson, A., Reyes, C., Sanay, R., 2003. Effects of bathymetry, friction, and rotation on estuary–ocean exchange. Journal of Physical Oceanography 33, 2375–2393.
Wang, D.P., 1979. Wind-induced circulation in the Chesapeake Bay, winter 1975. Journal of Physical Oceanography 9, 564–572.
Weisberg, R.H., 1976. The nontidal flow in the Providence River of Narragansett Bay: a stochastic approach to estuarine circulation. Journal of Physical Oceanography 6, 721–734.
Winant, C.D., 2004. Three-dimensional wind-driven flow in an elongated, rotating basin. Journal of Physical Oceanography 34, 462–476.
Wong, K.-C., 1994. On the nature of transverse variability in a coastal plain estuary. Journal of Geophysical Research 99, 14209–14222.
Wong, K.-C., Valle-Levinson, A., 2002. On the relative importance of the remote and local wind effects on the subtidal exchange at the entrance to the Chesapeake Bay. Journal of Marine Research 60, 477–498.